Sensitivity and Stability Analysis of The Trend of Sar-Cov-2 Infection with Time Delay Characterization

Peter Nwagor

Department of Mathematics, Ignatius Ajuru University of Education, Rivers State, Nigeria

Abstract

The study explores the dynamics of a COVID-19 epidemic in multiple susceptible populations, including the various stages of vaccination administration. In the model, there are eight human compartments: completely susceptible; susceptible with dose-1 vaccination; susceptible with dose-2 vaccination; susceptible with booster dose vaccination; exposed; infected with and without symptoms, and recovered compartments. The biological feasibility of the model is analysed. The threshold value, R_0, is derived using the next-generation matrix. The stability analysis of the equilibrium points was performed locally and globally using the threshold parameter of the model. The conditions determining disease persistence is obtained. The model is subjected to sensitivity analysis, and the most sensitive parameters are identified. Also, MATLAB is used to verify the mathematical outcomes of the system's dynamic behaviour and suggests that necessary steps should be taken to keep the spread of the omicron variant infectious disease under control. The findings of this study could aid health officials in their efforts to combat the spread of COVID-19.

Keywords: Boundedness; Basic reproduction number; Stability; Sensitivity; Vaccination

1. Introduction

SARS-CoV-2 or Coronavirus-19 was officially declared a global epidemic in March 2020, affecting and changing human life worldwide. It has only been recently that many countries have started investigating the origins of the new coronavirus. Some of its characteristics complicate the detection of epidemic breakouts; among them is the large number of people who are asymptomatic but can infect others. Furthermore, the number of hospitalised patients with COVID-19 increases asymmetrically with age; it is almost innocuous for teenagers and young adults. However, it is hazardous for the elderly, especially in conjunction with other conditions; it has caused more than 10^5
deaths in Italy, accounting for more than 3 million infections; The average age of COVID-19 patients who died

Italy was 81. Social distancing, face masks, lock-downs, self-isolation/quarantine, contact tracing, and vaccination administration are all effective techniques for avoiding the spread of this virus. The Centers for Disease Control and Prevention have designated this pandemic as a public health issue. Approximately six feet apart, droplets are the means of transmission caused by coughing, sneezing, and talking. The Spanish Flu (1918 to 1920) and the Ebola epidemic (2014 to 2016) are examples of historical pandemics that have impacted human health and economic development [1–4]

The Indian government has approved four vaccinations: Covishield, Covaxin, Sputnik V, and spikevax. The Indian government began vaccinating individuals with the help of the National Expert Group on COVID-19 Vaccine Administration (NEGVAC), intending to vaccinate 300 million people in 180 days and complete the process by August 2021. The vaccination was administered to people in three phases. The first phase vaccination programme, which began on January 16, 2021, was only for health and front-line workers and was completed by April 3, 2021. The phase two vaccination programme began on March 1, 2021, and was mainly for people over 45 years old with other health complications and 60+year-old adults. Finally, the Phase 3 vaccination programme was opened to all adults over 18 years on May 1, 2021, after the second wave hit the country in April 2021 [5–8].

There were many variants of COVID-19 as announced by WHO, namely the alpha variant spreading to many countries in late 2020, the variant beta(B.1.351) dominant in many parts of southern Africa, the Gamma variant (P.1) dominant in the U.S and Brazil in January 2021, the Delta variant (B.1.617.2) dominant in many countries including India from December 2020, variant Mu(B.1.621) dominant in South Africa and other countries from January 2021,

R.1 variant dominant in Japan in March 2021, omicron variant(B1.1.529) dominant in South Africa, India and U.S from November 2021 onwards [9].

A model for tracking and predicting the intensity of the virus is required to plan for future outbreaks and alert administrations and communities about what can be done today to prevent transmission and infection. We can model and track current outbreak trends to prepare for future breakouts. This measure will help prevent the next coronavirus outbreak from being as severe. Global health decisions are made better with mathematical models that allow us to understand epidemiological patterns. Epidemic transmission patterns remain challenging to predict because a mathematical system is contingent on the presence of its solutions. Data is frequently skewed, delayed, or erroneous, and obtaining quality data is one of the most challenging tasks. Furthermore, traditional epidemic models assume that epidemic transmission occurs without interventions, a rare event. Keeping track of daily activities and travel, which intertwine with the spread of infection, makes it more challenging. Furthermore, there are far too many occurrences in hospitals where the interaction rate is more significant than in the general population. This cannot be ignored anyhow. Another difficulty here is estimating the epidemic model's parameters. To fully understand, capture, and predict the transmission of infectious illnesses, epidemiologists must continue to use mathematical models. Recently, there has been much research and development into understanding and predicting COVID-19. Using mathematical formulations to model the transmission of infectious diseases like COVID-19 is a well-established approach to analysing individuals and their infections in communities. Several studies have been published examining the dynamics of the COVID-19 epidemic worldwide [14–28,30,32,35–39,41–50,52–55,57–83]. Vaccination's impact on the spread of COVID-19 has been the subject of several articles [40,51]. During the second wave of COVID-19, mathematical models involving multiple susceptible compartments with each susceptible compartment containing individuals at varying phases of vaccination were the least explored. We present a compartmental mathematical model that includes multiple susceptible compartments corresponding to distinct vaccination stages.

The mathematical model is described and formalised in Section 2. The Section 3 examines the model's essential characteristics. The system's equilibrium points are determined in Section 3.3, and the criteria for its existence are specified. The disease-free equilibrium is discussed in Section 4, and the endemic equilibrium point is examined in Section 5. A bifurcation analysis is conducted in Section 6. In Section 7, the sensitivity analysis is carried out, and the parameter with the most sensitivity index is identified. The parameter estimation is performed in Section 8. The numerical simulations are performed in Section 9 and finally, in Section 10, all of the results have been summarised.

2. Construction of novel COVID-19 model

The COVID-19 model's population is organised into eight classes, namely, the susceptible population without vaccination (S_0), the susceptible population vaccinated with dose 1 (S_1), the susceptible population vaccinated with dose 2 (S_2), susceptible population with a booster dose (S_3), exposed population (E), infected and asymptomatic population to omicron variant induced COVID-19 disease (I_A), infected and symptomatic population to omicron

variant induced COVID-19 disease (I_S) and the recovered population from omicron variant induced COVID-19 disease (R). The following assumptions are included in the model:

The total population $M = S_0 + S_1 + S_2 + S_3 + E + I_A + I_S + R$ is assumed to be constant, while the individual compartment populations vary over time. It is assumed that dose-1 vaccination is given to non-vaccinated susceptible individuals, dose-2 vaccination is given to dose-1 vaccinated susceptible individuals, and a booster dose vaccination is given to dose-2 vaccinated individuals. The omicron variant viral infection is assumed to exclusively affect those who have not had either dose-1 or dose-2 of vaccination, and it does not affect people who have received a booster dose. Individuals' disease-related deaths were assumed to occur mainly in the infected but symptomatic compartment, and only natural death occurs in the remaining compartments. It is assumed that when non-vaccinated individuals have contact with infected but asymptomatic individuals, they get exposed to the infection with the transmission coefficient given by $\beta_1 S_0 I_A$. When susceptible dose-1 vaccinated individuals have contact with infected but asymptomatic individuals, they get exposed to the infection with the transmission coefficient given by $\beta_2 S_1 I_A$. When susceptible dose-2 vaccinated individuals have contact with infected but asymptomatic individuals, they get exposed to the infection with the transmission coefficient given by $\beta_3 S_2 I_A$. It is assumed that those who recover will be immune to the disease for the rest of their lives. It is supposed that the people who are exposed to the infection are asymptomatic of the disease after testing positive for the disease and moves to an asymptomatic infected compartment with the transmission coefficient given by γE and following the appearance of symptoms, the infected individual transfers to the symptomatic infected compartment, with $\delta_1 I_A$ as the transmission coefficient. The individuals who are recovered from both asymptomatic and symptomatic infections due to supportive care treatments available for COVID-19 disease in hospitals under isolation are recovered and moved to the recovered compartment with a transmission coefficient given by $\delta_2 I_A$ and $\sigma_1 I_S$ respectively. Symptomatic infected individuals are assumed to be isolated and undergo supportive care treatments in hospitals, so these individuals do not spread the disease. The omicron variant-induced COVID-19 pandemic model is formulated as below.

$$\begin{aligned}
\dot{S_0} &= \Lambda - \beta_1 S_0 I_A - (\alpha_1 + \xi) S_0 .\\
\dot{S_1} &= \alpha_1 S_0 - \beta_2 S_1 I_A - (\alpha_2 + \xi) S_1 .\\
\dot{S_2} &= \alpha_2 S_1 - \beta_3 S_2 I_A - (\alpha_3 + \xi) S_2 .\\
\dot{S_3} &= \alpha_3 S_2 - \xi S_3 .\\
\dot{E} &= (\beta_1 S_0 + \beta_2 S_1 + \beta_3 S_2) I_A - (\gamma + \xi) E .\\
\dot{I_A} &= \gamma E - (\delta_1 + \delta_2 + \xi) I_A .\\
\dot{I_S} &= \delta_1 I_A - (\sigma_1 + \sigma_2 + \xi) I_S .\\
\dot{R} &= \delta_2 I_A + \sigma_1 I_S - \xi R .
\end{aligned} \tag{1}$$

The preliminary conditions are given by

$$0 < S_i(0) < \infty , 0 \le E(0), I_A(0), I_S(0), R(0) < \infty , i = 0, 1, 2, 3. \tag{2}$$

In our model, the flow diagram of the omicron virus transmission in the human population is presented in Fig. 1.

3. The fundamental characteristics of the model

3.1. The characteristic of non-negativity in solutions

It is essential to show that for all time $t \ge 0$, each solution of system (1) with preliminary conditions (2) remains non-negative.

Theorem 1. *For any $t \ge 0$, each solution of system (1) with preliminary conditions (2) is non-negative.*

Proof. Using the first equation of (1) with initial condition (2), we get

$$\dot{S_0} = \Lambda - (\beta_1 I_A + c_1) S_0 > -(\beta_1 I_A + c_1) S_0 . \tag{3}$$

As a result, after integrating, we obtain,

$$S_0(t) > S_0(0) e^{-\int_0^t (\beta_1 I_A + c_1) dt} > 0. \tag{4}$$

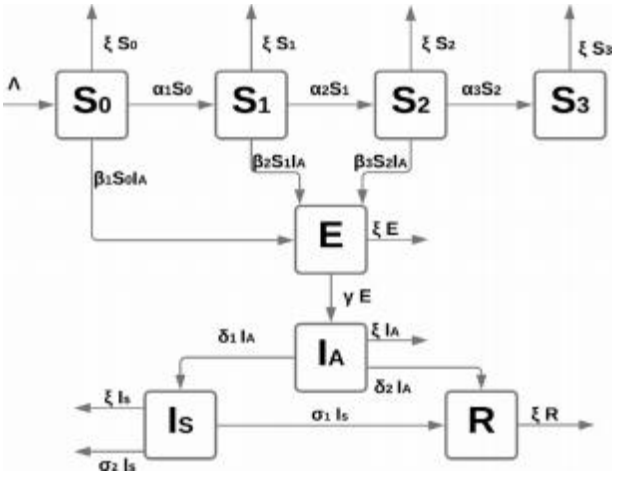

Fig. 1. Virus transmission diagram of the system (1).

Similarly from the remaining equations of (1) utilising the initial conditions (2), we get

$$\begin{aligned}
&S_1(t) > S_1(0)\, e^{-\int_0^t (\beta_2 I_A + c_2)dt} > 0,\\
&S_2(t) > S_2(0)\, e^{-\int_0^t (\beta_3 I_A + c_3)dt} > 0,\\
&S_3(t) > S_3(0)\, e^{-\xi t} > 0,\\
&E(t) \geq E(0)\, e^{-c_4 t} \geq 0,\\
&I_A(t) \geq I_A(0)\, e^{-c_5 t} \geq 0,\\
&I_S(t) \geq I_S(0)\, e^{-c_6 t} \geq 0,\\
&R(t) \geq R(0)\, e^{-\xi t} \geq 0.
\end{aligned} \tag{5}$$

where $c_1 = \alpha_1 + \xi$, $c_2 = \alpha_2 + \xi$, $c_3 = \alpha_3 + \xi$, $c_4 = \gamma + \xi$, $c_5 = \delta_1 + \delta_2 + \xi$, $c_6 = \sigma_1 + \sigma_2 + \xi$. Hence, $0 < S_i(t) < \infty$, $0 \leq E(t)$, $I_A(t)$, $I_S(t)$, $R(t) < \infty$, $i = 0, 1, 2, 3$. □

3.2. Invariant region and uniform boundedness of solutions

We will now prove that all of system (1)'s solutions are bounded uniformly and there exist solutions to system (1) of $\mathbb{R}^8_+$ in a positively invariant region.

Theorem 2. *The system (1)'s solutions with preliminary conditions (2) are bounded uniformly in* $\mathbb{R}^8_+$ *and are confined to the region* $\Delta = \{(S_0, S_1, S_2, S_3, E, I_A, I_S, R) \in \mathbb{R}^8_+ : 0 < M \leq \frac{\Lambda}{\xi}\}$ *as* $t \to \infty$, *where* $M = S_0 + S_1 + S_2 + S_3 + E + I_A + I_S + R$.

Proof. Let $M = S_0 + S_1 + S_2 + S_3 + E + I_A + I_S + R$, where $M = M(t)$ is the total population at time t. For $m > 0$ we have,

$$\frac{dM}{dt} + mM = \Lambda - (\xi - m) - \sigma_2 I_S \leq \Lambda. \tag{6}$$

if and only if $m \leq \xi$. Using differential inequality theory [31], we can arrive at the following conclusion:

$$0 < M \leq \frac{\Lambda}{m}\left(1 - e^{-mt}\right) + M(0)e^{-mt}. \tag{7}$$

which yields $0 < M \leq \frac{\Lambda}{m}$ as $t \to \infty$ with $m \leq \xi$. Hence system (1)'s solutions with preliminary conditions (2) starting in $\mathbb{R}^8_+$ are bounded uniformly and limited to the region $\Delta = \{(S_0, S_1, S_2, S_3, E, I_A, I_S, R) \in \mathbb{R}^8_+ : 0 <$

$M(t) \leq \frac{\Lambda}{m}\}$, where $m \leq \xi$. As a result, the closed region Δ is positively invariant, and all system (1)'s solutions are bounded uniformly. □

Remark 1. All of system (1)'s solutions with preliminary conditions (2) have non-negative components in Δ for $t \geq 0$ and are globally attracted in R_+^8. As a result, the system (1) with preliminary conditions (2) defined on $\Delta = \{(S_0, S_1, S_2, S_3, E, I_A, I_S, R) \in R_+^8 : 0 < M(t) \leq \frac{\Lambda}{m}\}$, where $m \leq \xi$ is well-posed mathematically and epidemiologically. We will investigate the dynamics of system (1) without the recovered compartment defined on the invariant region $\Delta = \{(S_0, S_1, S_2, S_3, E, I_A, I_S) \in R_+^7 : 0 < M(t) \leq \frac{\Lambda}{m}\}$, where $m \leq \xi$, because the recovered compartment of individuals is independent of other compartments.

3.3. The system's equilibrium points

The equilibrium points for the system (1) are as follows

1. Disease free equilibrium (DFE) point $P_0 = (S_0^0, S_1^0, S_2^0, S_3^0, E^0, I_A^0, I_S^0)$, where, $S_0^0 = \frac{\Lambda}{c_1}$, $S_1^0 = \frac{\Lambda\alpha_1}{c_1c_2}$, $S_2^0 = \frac{\Lambda\alpha_1\alpha_2}{c_1c_2c_3}$, $S_3^0 = \frac{\Lambda\alpha_1\alpha_2\alpha_3}{\xi c_1c_2c_3}$, $E^0 = 0$, $I_A^0 = 0$, $I_S^0 = 0$. Here, $c_1 = \alpha_1 + \xi$, $c_2 = \alpha_2 + \xi$, $c_3 = \alpha_3 + \xi$, $c_4 = \gamma + \xi$, $c_5 = \delta_1 + \delta_2 + \xi$, $c_6 = \sigma_1 + \sigma_2 + \xi$
2. Endemic equilibrium (EE) point $P_1 = (S_0^*, S_1^*, S_2^*, S_3^*, E^*, I_A^*, I_S^*)$, where $S_0^* = \frac{\Lambda}{c_1+\beta_1 I_A^*}$, $S_1^* = \frac{\Lambda\alpha_1}{(c_1+\beta_1 I_A^*)(c_2+\beta_2 I_A^*)}$, $S_2^* = \frac{\Lambda\alpha_1\alpha_2}{(c_1+\beta_1 I_A^*)(c_2+\beta_2 I_A^*)(c_3+\beta_3 I_A^*)}$, $S_3^* = \frac{\Lambda\alpha_1\alpha_2\alpha_3}{(c_1+\beta_1 I_A^*)(c_2+\beta_2 I_A^*)(c_3+\beta_3 I_A^*)\xi}$ $E^* = \frac{[\beta_2\beta_3(\alpha_1+I_A^*\beta_1)+\alpha_1\alpha_2\beta_3+(\alpha_1+I_A^*\beta_1)\beta_2\beta_3 I_A^*+c_2\beta_1(\beta_3+I_A^*\beta_3)]+\Lambda I_A^*}{c_4(c_1+\beta_1 I_A^*)(c_2+\beta_2 I_A^*)(c_3+\beta_3 I_A^*)}$, $I_S^* = \frac{\delta_1 I_A^*}{c_6}$ From the sixth equation of (1) after simplification, we get the polynomial equation

$$k_3 I_A^{*3} + k_2 I_A^{*2} + k_1 I_A^* + k_0 = 0. \tag{8}$$

where

$$\begin{aligned} k_0 &= c_1c_2c_3c_4c_5\left[1 - \frac{(c_2c_3\beta_1 + c_3\alpha_1\beta_2 + \alpha_1\alpha_2\beta_3)\Lambda\gamma}{c_1c_2c_3c_4c_5}\right], \\ k_1 &= c_4c_5\left[c_2c_3\beta_1 + c_1c_3\beta_2 + c_1c_2\beta_3\right] - \gamma\Lambda\left[c_3\beta_1\beta_2 + c_2\beta_1\beta_3 + \alpha_1\beta_2\beta_3\right], \\ k_2 &= c_4c_5\left[c_3\beta_1\beta_2 + c_2\beta_1\beta_3 + c_1\beta_2\beta_3\right] - \beta_1\beta_2\beta_3\gamma\Lambda, \\ k_3 &= c_4c_5\beta_1\beta_2\beta_3. \end{aligned} \tag{9}$$

Clearly, $k_3 > 0$ and if we set $R_0 = \frac{(c_2c_3\beta_1+c_3\alpha_1\beta_2+\alpha_1\alpha_2\beta_3)\Lambda\gamma}{c_1c_2c_3c_4c_5}$, then $k_0 < 0$ whenever $R_0 > 1$. The above polynomial in I_A^* has three roots and by Descartes rule of sign, the polynomial has either one or three positive real roots for all possible combination of signs of k_1 and k_2. As a result, the polynomial (8) always has at least one positive root if $R_0 > 1$. Hence if $R_0 > 1$ then $I_A^* > 0$ always and hence S_0^*, S_1^*, S_2^*, S_3^*, E^*, I_S^* belong to R^+. As a result P_1 always exists if $R_0 > 1$.

4. Stability analysis on DFE

4.1. Next generation matrix method

The mean number of secondary infections induced by a single infection is known as the Basic Reproduction Number (BRN). It is one of the most important threshold values for mathematically expressing a virus infection's spread.

At a given point $P = (S_0, S_1, S_2, S_3, E, I_A, I_S)$, the Jacobian matrix of the system (1) is given by $J(P)$ as follows:

$$J(P) = \begin{pmatrix} -(\beta_1 I_A + c_1) & 0 & 0 & 0 & 0 & -\beta_1 S_0 & 0 \\ \alpha_1 & -(\beta_2 I_A + c_2) & 0 & 0 & 0 & -\beta_2 S_1 & 0 \\ 0 & \alpha_2 & -(\beta_3 I_A + c_3) & 0 & 0 & -\beta_3 S_2 & 0 \\ 0 & 0 & \alpha_3 & -\xi & 0 & 0 & 0 \\ \beta_1 I_A & \beta_2 I_A & \beta_3 I_A & 0 & -c_4 & (\beta_1 S_0 + \beta_2 S_1 + \beta_3 S_2) & 0 \\ 0 & 0 & 0 & 0 & \gamma & -c_5 & 0 \\ 0 & 0 & 0 & 0 & 0 & \delta_1 & -c_6 \end{pmatrix}, \tag{10}$$

P_0's stability corresponds to eigenvalues of $J(P)$'s characteristic equation at P_0 being of negative real parts, as confirmed by the BRN computed using the next-generation matrix approach. Let us assume $x = (E, I_A, I_S, S_0, S_1, S_2, S_3)^T$ and hence the system (1) is expressed as

$$x. = \mathsf{F} - \mathsf{V}. \tag{11}$$

where

$$\mathcal{F}(x) = \begin{pmatrix} \beta_1 S_0 + \beta_2 S_1 + \beta_3 S_2 \\ 0 \\ 0 \\ 0 \\ 0 \\ 0 \\ 0 \end{pmatrix},$$

and

$$\mathsf{V}(x) = \begin{pmatrix} c_4 E \\ -\gamma E + c_5 I_A \\ -\delta_1 I_A + c_6 I_S \\ -\Lambda + \beta_1 S_0 I_A + c_1 S_0 \\ -\alpha_1 S_0 + \beta_2 S_1 I_A + c_2 S_1 \\ -\alpha_2 S_1 + \beta_3 S_2 I_A + c_3 S_2 \\ -\alpha_3 S_2 + \xi S_3 \end{pmatrix}.$$

The Jacobian matrices of $\mathsf{F}(x)$ and $\mathsf{V}(x)$ at P_0 are as follows.

$$F = \begin{pmatrix} 0 & \frac{\Lambda(\beta_1 c_2 c_3 + \beta_2 \alpha_1 c_3 + \beta_3 \alpha_1 \alpha_2)}{c_1 c_2 c_3} & 0 \\ 0 & 0 & 0 \\ 0 & 0 & 0 \end{pmatrix}$$

and

$$V = \begin{pmatrix} c_4 & 0 & 0 \\ -\gamma & c_5 & 0 \\ 0 & -\delta_1 & c_6 \end{pmatrix}.$$

The next generation matrix for system (1)is given by

$$F\ V^{-1} = \begin{pmatrix} \frac{\gamma \Lambda(\beta_1 c_2 c_3 + \beta_2 \alpha_1 c_3 + \beta_3 \alpha_1 \alpha_2)}{c_1 c_2 c_3 c_4 c_5} & \frac{(\beta_1 c_2 c_3 + \beta_2 \alpha_1 c_3 + \beta_3 \alpha_1 \alpha_2)\Lambda}{c_1 c_2 c_3 c_5} & 0 \\ 0 & 0 & 0 \\ 0 & 0 & 0 \end{pmatrix}$$

The spectral radius $\rho\ (F\ V^{-1})$ of $F\ V^{-1}$ is the BRN given as follows:

$$R_0 = \frac{\gamma \Lambda(\beta_1 c_2 c_3 + \beta_2 \alpha_1 c_3 + \beta_3 \alpha_1 \alpha_2)}{c_1 c_2 c_3 c_4 c_5}. \tag{12}$$

where $c_1 = \alpha_1 + \xi$, $c_2 = \alpha_2 + \xi$, $c_3 = \alpha_3 + \xi$, $c_4 = \gamma + \xi$, $c_5 = \delta_1 + \delta_2 + \xi$.

4.2. The analysis of P_0's local stability

In this part, we investigate the local asymptotic stability (LAS) of the disease-free equilibrium point P_0.

Theorem 3. *The point P_0 of system (1) is LAS whenever $R_0 < 1$ and is unstable if $R_0 > 1$.*

Proof. The jacobian matrix evaluated at P_0 of the system (1) is

$$J(P_0) = \begin{pmatrix} -c_1 & 0 & 0 & 0 & 0 & \frac{-\beta_1 \Lambda}{c_1} & 0 \\ \alpha_1 & -c_2 & 0 & 0 & 0 & \frac{-\beta_2 \alpha_1 \Lambda}{c_1 c_2} & 0 \\ 0 & \alpha_2 & -c_3 & 0 & 0 & \frac{-\beta_3 \Lambda \alpha_1 \alpha_2}{c_1 c_2 c_3} & 0 \\ 0 & 0 & \alpha_3 & -\xi & 0 & 0 & 0 \\ 0 & 0 & 0 & 0 & -c_4 & \left(\frac{\beta_1 \Lambda}{c_1} + \frac{\beta_2 \alpha_1 \Lambda}{c_1 c_2} + \frac{\beta_3 \alpha_1 \alpha_2 \Lambda}{c_1 c_2 c_3}\right) & 0 \\ 0 & 0 & 0 & 0 & \gamma & -c_5 & 0 \\ 0 & 0 & 0 & 0 & 0 & \delta_1 & -c_6 \end{pmatrix} \tag{13}$$

$J(P_0)$ has the following characteristic equation

$$|J(P_0) - \lambda I| = 0. \tag{14}$$

Hence, we get the polynomial in λ, say

$$(\lambda + c_1)(\lambda + \xi)(\lambda + c_2)(\lambda + c_6)(\lambda + c_3)\,[(c_2 c_3 \beta_1 + c_3 \alpha_1 \beta_2 + \alpha_1 \alpha_2 \beta_3)\gamma\Lambda - c_1 c_2 c_3 (\lambda + c_4)(\lambda + c_5)] = 0. \tag{15}$$

The five eigen values of the characteristic equation are given by $\lambda = -c_1 < 0$, $\lambda = -\xi$, $\lambda = -c_2 < 0$, $\lambda = -c_6 < 0$ and $\lambda = -c_3 < 0$. The remaining two eigen values of the characteristic equation are given by the equation

$$(c_2 c_3 \beta_1 + c_3 \alpha_1 \beta_2 + \alpha_1 \alpha_2 \beta_3)\gamma\Lambda - c_1 c_2 c_3 (\lambda + c_4)(\lambda + c_5) = 0. \tag{16}$$

After simplifying the above equation, we get

$$\lambda^2 + a_1 \lambda + a_2 = 0. \tag{17}$$

where

$$\begin{aligned} a_1 &= c_4 + c_5. \\ a_2 &= c_4 c_5 \left(1 - \frac{(c_2 c_3 \beta_1 + c_3 \alpha_1 \beta_2 + \alpha_1 \alpha_2 \beta_3)\gamma \Lambda}{c_1 c_2 c_3 c_4 c_5}\right) \\ &= c_4 c_5 (1 - R_0). \end{aligned} \tag{18}$$

Clearly $a_1 > 0$ but $a_2 > 0$ if and only if $R_0 < 1$. Hence, P_0 is LAS if $R_0 < 1$ and unstable if $R_0 > 1$ according to Hurwitz–Routh criterion [29]. □

4.3. The analysis of P_0'sglobal stability

We analyse the global asymptotic stability (GAS) of P_0 based on the value of R_0 using the conditions in Castillo-Chavez method [34] in this section. To prove the GAS of P_0, the feasible region $\Delta_1 = \{(S_0, S_1, S_2, S_3, E, I_A, I_S) \in \Delta : S_0 \le S_0^0, S_1 \le S_1^0, S_2 \le S_2^0\}$ is used. Firstly, the region Δ_1's positively invariant property is established.

Theorem 4. *For the omicron system (1), the region* $\Delta_1 = \{(S_0, S_1, S_2, S_3, E, I_A, I_S) \in \Delta : S_0 \le S_0^0, S_1 \le S_1^0, S_2 \le S_2^0\}$ *is a positively invariant set.*

Proof. From system (1), we obtain

$$\begin{aligned} \dot{S_0} &= \Lambda - \beta_1 S_0 I_A - c_1 S_0 \\ &\le \Lambda - c_1 S_0. \end{aligned} \tag{19}$$

Hence we get,

$$S_0(t) \le S_0^0 - (S_0^0 - S_0(0))e^{-c_1 t}. \tag{20}$$

If $S_0(0) \in \Delta_1$, then $S_0(0) \le S_0^0$. Therefore $S_0(t) \le S_0^0 - (S_0^0 - S_0(0))e^{-c_1 t} \le S_0^0 \ \forall\, t \ge 0$. Similarly, we deduce from second and third equations of system (1), $S_1(t) \le S_1^0$ and $S_2(t) \le S_2^0$, $\forall\, t \ge 0$ if the initial conditions $S_i(0) \in \Delta_1$ for $i = 1, 2$. As a result, the region Δ_1 is positively invariant set which attracts all of the system (1) solutions in $\mathbb{R}_+^7$. □

Theorem 5. *If $R_0 < 1$, P_0 is GAS in Δ_1.*

Proof. The system (1) is written as

$$\begin{aligned} X' &= K(X, I). \\ I' &= L(X, I). \end{aligned} \tag{21}$$

Where, dot denotes differentiation with respect to t in this context and $X = (S_0, S_1, S_2, S_3)^T$, $I = (E, I_A, I_S)^T$,

$$K(X,I) = \begin{pmatrix} \Lambda - \beta_1 S_0 I_A - c_1 S_0 \\ \alpha_1 S_0 - \beta_2 S_1 I_A - c_2 S_1 \\ \alpha_2 S_1 - \beta_3 S_2 I_A - c_3 S_2 \\ \alpha_3 S_2 - \xi S_3 \end{pmatrix}, \qquad L(X,I) = \begin{pmatrix} (\beta_1 S_0 + \beta_2 S_1 + \beta_3 S_2) I_A - c_4 E \\ \gamma E - c_5 I_A \\ \delta_1 I_A - c_6 I_S \end{pmatrix}$$

Furthermore

$$A = \begin{pmatrix} -c_4 & \beta_1 S_0^0 + \beta_2 S_1^0 + \beta_3 S_2^0 & 0 \\ \gamma & -c_5 & 0 \\ 0 & \delta_1 & -c_6 \end{pmatrix}, \quad \hat{L}(X,I) = \begin{pmatrix} [\beta_1 (S_0^0 - S_0) + \beta_2 (S_1^0 - S_1) + \beta_3 (S_2^0 - S_2)] I_A \\ 0 \\ 0 \end{pmatrix},$$

$$K(X,I)\Big|_{I=0} = \begin{pmatrix} \Lambda - c_1 S_0 \\ \alpha_1 S_0 - c_2 S_1 \\ \alpha_2 S_1 - c_3 S_2 \\ \alpha_3 S_2 - \xi S_3 \end{pmatrix}, \; L(X,I)\Big|_{I=0} = \begin{pmatrix} 0 \\ 0 \\ 0 \end{pmatrix}, \text{ where } A = D_I L(X^*, 0), \quad L(X,I) = AI - \hat{L}(X,I)$$

Solving the system $\frac{dX}{dt} = K(X, 0)$, we get $S_0(t) = \frac{\Lambda}{c_1} + (S_0(0) - \frac{\Lambda}{c_1}) e^{-c_1 t}$ and hence $\lim_{t\to\infty} S_0(t) = S_0^0$ and similarly from the other equations of $\frac{dX}{dt} = K(X, 0)$, we get $\lim_{t\to\infty} S_1(t) = S_1^0$, $\lim_{t\to\infty} S_2(t) = S_2^0$ and $\lim_{t\to\infty} S_3(t) = S_3^0$. The solutions of $\frac{dX}{dt} = K(X, 0)$ do not depend on the initial conditions $S_i(0)$, $i = 0, 1, 2, 3$. As a result, the asymptotic nature of the solutions $S_i(t)$, $i = 0, 1, 2, 3$ is independent of the preliminary conditions in Δ_1, ensuring the global asymptotic stability of the equilibrium point $X^* = (\frac{\Lambda}{c_1}, \frac{\alpha_1 \Lambda}{c_1 c_2}, \frac{\alpha_1 \alpha_2 \Lambda}{c_1 c_2 c_3}, \frac{\Lambda \alpha_1 \alpha_2 . \alpha_3}{\xi c_1 c_2 c_3})$ and hence the first condition of the Castillo-Chavez method [34] is satisfied. Further in Δ_1, $S_0 \le S_0^0$, $S_1 \le S_1^0$, $S_2 \le S_2^0$ and hence

$$\beta_1 (S_0^0 - S_0) + \beta_2 (S_1^0 - S_1) + \beta_3 (S_2^0 - S_2) \ge 0. \tag{22}$$

This implies that

$$\hat{L}(X, I) \ge 0. \tag{23}$$

which satisfies the second condition of the Castillo-Chavez method [34]. As a result, P_0 is GAS if $R_0 < 1$. □

5. Stability analysis of EE

In this section, we analyse the local asymptotic stability (LAS) and global asymptotic stability (GAS) of the endemic equilibrium (EE) point P_1.

5.1. The analysis of P_1's local stability

Theorem 6. *The EE point P_1 of the system (1) is LAS if $R_0 > 1$ and all of the conditions in the proof are met.*

Proof. The Jacobian matrix of system (1) at P_1 is

$$J(P_1) = \begin{pmatrix} -(c_1 + \beta_1 I_A^*) & 0 & 0 & 0 & 0 & -\beta_1 S_0^* & 0 \\ \alpha_1 & -(c_2 + \beta_2 I_A^*) & 0 & 0 & 0 & -\beta_2 S_1^* & 0 \\ 0 & \alpha_2 & -(c_3 + \beta_3 I_A^*) & 0 & 0 & -\beta_3 S_2^* & 0 \\ 0 & 0 & \alpha_3 & -\xi & 0 & 0 & 0 \\ \beta_1 I_A^* & \beta_2 I_A^* & \beta_3 I_A^* & 0 & -c_4 & \beta_1 S_0^* + \beta_2 S_1^* + \beta_3 S_2^* & 0 \\ 0 & 0 & 0 & 0 & \gamma & -c_5 & 0 \\ 0 & 0 & 0 & 0 & 0 & \delta_1 & -c_6 \end{pmatrix}, \tag{24}$$

The determinantal equation of (24) is given by

$$|J(P_1) - \tau I| = 0. \tag{25}$$

Hence we get the polynomial in τ, say

$$(\tau + c_6)(\tau + \xi)(\tau^5 + B_1\tau^4 + B_2\tau^3 + B_3\tau^2 + B_4\tau + B_5) = 0. \tag{26}$$

The two latent roots of (26) are $\tau = -c_6 < 0$ and $\tau = -\xi < 0$. The remaining latent roots of (26) are analysed using the polynomial equation

$$\tau^5 + B_1\tau^4 + B_2\tau^3 + B_3\tau^2 + B_4\tau + B_5 = 0. \tag{27}$$

The coefficients of (27) are as follows:

$$B1 = c_1 + c_2 + c_3 + c_4 + c_5 + I_A^*(\beta 1 + \beta 2 + \beta 3) > 0.$$

$$B2 = c_3c_4 + c_3c_5 + c_3I_A^*\beta 1 + c_4I_A^*\beta 1 + c_5I_A^*\beta 1 + c_3I_A^*\beta 2 + c_4I_A^*\beta 2 + c_5I_A^*\beta 2 + I_A^{*2}\beta 1\beta 2 + c_4I_A^*\beta 3 + c_5I_A^*\beta 3 + I_A^{*2}\beta 1\beta 3 + I_A^{*2}\beta 2\beta 3 + c_2(c_3 + c_4 + c_5 + I_A^*(\beta 1 + \beta 3)) + c_1(c_2 + c_3 + c_4 + c_5 + I_A^*(\beta 2 + \beta 3)) > 0.$$

$$B3 = c_1c_2c_3 + c_1c_2c_4 + c_1c_3c_4 + c_2c_3c_4 + c_1c_2c_5 + c_1c_3c_5 + c_2c_3c_5 + c_2c_3I_A^*\beta 1 + c_2c_4I_A^*\beta 1 + c_3c_4I_A^*\beta 1 + c_2c_5I_A^*\beta 1 + c_3c_5I_A^*\beta 1 + I_A^*S_0^*\gamma\beta_1^2 + c_1c_3I_A^*\beta 2 + c_1c_4I_A^*\beta 2 + c_3c_4I_A^*\beta 2 + c_1c_5I_A^*\beta 2 + c_3c_5I_A^*\beta 2 + I_A^*S_1^*\gamma\beta_2^2 + c_3I_A^{*2}\beta 1\beta 2 + c_4I_A^{*2}\beta 1\beta 2 + c_5I_A^{*2}\beta 1\beta 2 + c_1c_2I_A^*\beta 3 + c_1c_4I_A^*\beta 3 + c_2c_4I_A^*\beta 3 + c_1c_5I_A^*\beta 3 + c_2c_5I_A^*\beta 3 + I_A^*S_2^*\gamma\beta_3^2 + c_2I_A^{*2}\beta 1\beta 3 + c_4I_A^{*2}\beta 1\beta 3 + c_5I_A^{*2}\beta 1\beta 3 + c_1I_A^{*2}\beta 2\beta 3 + c_4I_A^{*2}\beta 2\beta 3 + c_5I_A^{*2}\beta 2\beta 3 + I_A^{*3}\beta 1\beta 2\beta 3 > 0.$$

$$B4 = c_1c_2c_3c_4 + c_1c_2c_3c_5 + c_2c_3c_4I_A^*\beta 1 + c_2c_3c_5I_A^*\beta 1 + c_2I_A^*\beta_1^2S_0^*\gamma + c_3I_A^*\beta_1^2S_0^*\gamma + c_1c_3c_4I_A^*\beta 2 + c_1c_3c_5I_A^*\beta 2 + c_1I_A^*\beta_2^2S_1^*\gamma + c_3I_A^*\beta_2^2S_1^*\gamma + c_3c_4I_A^{*2}\beta 1\beta 2 + c_3c_5I_A^{*2}\beta 1\beta 2 + I_A^{*2}\beta 1\beta 2\gamma(S_0^*\beta 1 + S_1^*\beta 2) + c_1c_2c_4I_A^*\beta 3 + c_1c_2c_5I_A^*\beta 3 + c_1I_A^*\beta_3^2S_2^*\gamma + c_2I_A^*\beta_3^2S_2^*\gamma + c_2c_4I_A^{*2}\beta 1\beta 3 + c_2c_5I_A^{*2}\beta 1\beta 3 + I_A^{*2}\beta 1\beta 3\gamma(S_0^*\beta 1 + S_2^*\beta 3) + c_1c_4I_A^{*2}\beta 2\beta 3 + c_1c_5I_A^{*2}\beta 2\beta 3 + I_A^{*2}\beta 2\beta 3\gamma(S_1^*\beta 2 + S_2^*\beta 3) + c_4I_A^{*3}\beta 1\beta 2\beta 3 + c_5I_A^{*3}\beta 1\beta 2\beta 3 + I_A^*S_0^*\alpha 1\beta 1\beta 2\gamma + I_A^*S_1^*\alpha 2\beta 2\beta 3\gamma > 0.$$

$$B5 = c_4c_5I_A^{*3}\beta 1\beta 2\beta 3 + I_A^{*2}(c_3\beta 1\beta 2\gamma(S_0^*\beta 1 + S_1^*\beta 2) + c_2\beta 1\beta 3\gamma(S_0^*\beta 1 + S_2^*\beta 3) + c_1\beta 2\beta 3(S_1^*\beta 2 + S_2^*\beta 3)\gamma + (S_0^*\alpha 1 + S_1^*\alpha 2)\beta 1\beta 2\beta 3\gamma) + I_A(S_0^*\alpha 1\beta 1(c_3\beta 2 + \alpha 2\beta 3)\gamma + c_1c_2\beta 3(S_2^*\beta 3\gamma) + c_1\beta 2(c_3S_1^*\beta 2\gamma + S_1^*\alpha 2\beta 3\gamma) + c_2c_3\beta_1^2S_0^*\gamma) > 0.$$

The Hurwitz–Routh criterion [29] states that the polynomial (27) has all five roots be either negative or have roots with negative real parts if and only if the determinants of all Hurwitz matrices H_1, H_2, H_3, H_4, H_5 are positive, i.e.,

$$|H_i| > 0 \quad \text{for} \quad i = 1, 2, 3, 4, 5. \tag{28}$$

where $H_1 = (B_1)$, $H_2 = \begin{pmatrix} B_1 & 1 \\ B_3 & B_2 \end{pmatrix}$, $H_3 = \begin{pmatrix} B_1 & 1 & 0 \\ B_3 & B_2 & B_1 \\ B_5 & B_4 & B_3 \end{pmatrix}$, $H_4 = \begin{pmatrix} B_1 & 1 & 0 & 0 \\ B_3 & B_2 & B_1 & 1 \\ B_5 & B_4 & B_3 & B_2 \\ 0 & 0 & B_5 & B_4 \end{pmatrix}$ and

$$H_5 = \begin{pmatrix} B_1 & 1 & 0 & 0 & 0 \\ B_3 & B_2 & B_1 & 1 & 0 \\ B_5 & B_4 & B_3 & B_2 & B_1 \\ 0 & 0 & B_5 & B_4 & B_3 \\ 0 & 0 & 0 & 0 & B_5 \end{pmatrix}$$

The determinants of the Hurwitz matrices are given as follows:

$$|H_1| = B_1.$$

$$|H_2| = B_1B_2 - B_3.$$

$$|H_3| = -B_3^2 - B_1^2B_4 + B_1(B_2B_3 + B_5). \tag{29}$$

$$|H_4| = -B_4(-B_1B_2B_3 + B_3^2 + B_1^2B_4) + (-B_1B_2^2 + B_2B_3 + 2B_1B_4)B_5 - B_5^2.$$

$$|H_5| = -B_5(B_4(-B_1B_2B_3 + B_3^2 + B_1^2B_4) - B_2B_3B_5 + B_1(B_2^2 - 2B_4)B_5 + B_5^2).$$

But the EE point P_1 exists if $R_0 > 1$ and hence P_1 is LAS if $R_0 > 1$ and satisfies the conditions $|H_i| > 0$, $i = 1, 2, 3, 4, 5$. □

5.2. The analysis of P_1'sglobal stability

In this part, the global asymptotic stability (GAS) of endemic equilibrium (EE) point is analysed.

Theorem 7. *If $R_0 > 1$, the EE point P_1 is GAS if $P < Q$. The expressions of P and Q are specified in the proof.*

Proof. Let us create a suitable Lyapunov function as follows:

$$\begin{aligned} L(S_0, S_1, S_2, S_3, E, I_A, I_S) = {} & [S_0 - S_0^* + S_0^* \log(\frac{S_0^*}{S_0})] + [S_1 - S_1^* + S_1^* \log(\frac{S_1^*}{S_1})] + [S_2 - S_2^* + S_2^* \log(\frac{S_2^*}{S_2})] \\ & + [S_3 - S_3^* + S_3^* \log(\frac{S_3^*}{S})] + [E - E^* + E^* \log(\frac{E^*}{E})] + [I_A - I_A^* + I_A^* \log(\frac{I_A^*}{I_A})] \\ & + [I_S - I_S^* + I_S^* \log(\frac{I_S^*}{I_S})]. \end{aligned} \tag{30}$$

Then

$$\begin{aligned} \frac{dL}{dt} = {} & (\frac{S_0 - S_0^*}{S_0})\frac{dS_0}{dt} + (\frac{S_1 - S_1^*}{S_1})\frac{dS_1}{dt} + (\frac{S_2 - S_2^*}{S_2})\frac{dS_2}{dt} + (\frac{S_3 - S_3^*}{S_3})\frac{dS_3}{dt} \\ & + (\frac{E - E^*}{E})\frac{dE}{dt} + (\frac{I_A - I_A^*}{I_A})\frac{dI_A}{dt} + (\frac{I_S - I_S^*}{I_S})\frac{dI_S}{dt} \\ = {} & (\Lambda - \beta_1 S_0 I_A - c_1 S_0)(\frac{S_0 - S_0^*}{S_0}) + (\alpha_1 S_0 - \beta_2 S_1 I_A - c_2 S_1)(\frac{S_1 - S_1^*}{S_1}) \\ & + (\alpha_2 S_1 - \beta_3 S_2 I_A - c_3 S_2)(\frac{S_2 - S_2^*}{S_2}) + (\alpha_3 S_2 - \xi S_3)(\frac{S_3 - S_3^*}{S_3}) \\ & + ((\beta_1 S_0 + \beta_2 S_1 + \beta_3 S_2) I_A - c_4 E)(\frac{E - E^*}{E}) + (\gamma E - c_5 I_A)(\frac{I_A - I_A^*}{I_A}) + (\delta_1 I_A - c_6 I_S)(\frac{I_S - I_S^*}{I_S}). \end{aligned} \tag{31}$$

Using the endemic equilibrium point P_1 in (1), we get,

$$\begin{aligned} \Lambda - \beta_1 S_0^* I_A^* - c_1 S_0^* &= 0. \\ \alpha_1 S_0^* - \beta_2 S_1^* I_A^* - c_2 S_1^* &= 0. \\ \alpha_2 S_1^* - \beta_3 S_2^* I_A^* - c_3 S_2^* &= 0. \\ \alpha_3 S_2^* - \xi S_3^* &= 0. \\ (\beta_1 S_0^* + \beta_2 S_1^* + \beta_3 S_2^*) I_A^* - c_4 E^* &= 0. \\ \gamma E^* - c_5 I_A^* &= 0. \\ \delta_1 I_A^* - c_6 I_S^* &= 0. \end{aligned} \tag{32}$$

and using (32) in (31), we get,

$$\frac{dL}{dt} = P - Q. \tag{33}$$

where

$$\begin{aligned} P = {} & [\beta_1(I_A^* S_0 + I_A S_0^*) + \beta_2(I_A^* S_1 + I_A S_1^*) + \frac{\alpha_1}{S_1}(S_0 S_1 + S_0^* S_1^*) + \frac{\alpha_2}{S_2}(S_1 S_2 + S_1^* S_2^*) \\ & + \frac{\beta_3 S_2^*}{S_2}(I_A S_2^* + I_A^* S_2) + \frac{\alpha_3}{S_3}(S_2 S_3 + S_2^* S_3^*) + (\beta_1 S_0 + \beta_2 S_1 + \beta_3 S_2) I_A \\ & + \frac{I_A^* E^*}{E}(\beta_1 S_0^* + \beta_2 S_1^* + \beta_3 S_2^*) + \frac{\gamma}{I_A}(E I_A + E^* I_A^*) + \frac{\delta_1}{I_S}(I_A I_S + I_A^* I_S^*)]. \end{aligned}$$

$$
\begin{aligned}
Q = {} & [(S_0 - S_0^*)^2 \left(\frac{\beta_1 I_A^* + c_1}{S_0}\right) + \beta_1 (I_A^* S_0^* + I_A S_0) + (S_1 - S_1^*)^2 \left(\frac{\beta_2 I_A^* + c_2}{S_1}\right) \\
& + \beta_2 (I_A^* S_1^* + I_A S_1) + \frac{\alpha_1}{S_1}(S_0 S_1^* + S_1 S_0^*) + (S_2 - S_2^*)^2 \left(\frac{\beta_3 I_A^* + c_3}{S_2}\right) \\
& + \frac{\alpha_2}{S_2}(S_1 S_2^* + S_2 S_1^*) + \frac{\beta_3 S_2^*}{S_2}(I_A S_2 + I_A^* S_2^*) + \frac{\xi}{S_3}(S_3 - S_3^*)^2 + \frac{\alpha_3}{S_3}(S_2 S_3^* + S_2^* S_3) \\
& + \frac{c_4}{E}(E - E^*)^2 + \frac{I_A E^*}{E}(\beta_1 S_0 + \beta_2 S_1 + \beta_3 S_2) + (\beta_1 S_0^* + \beta_2 S_1^* + \beta_3 S_2^*) I_A^* + \frac{c_5}{I_A}(I_A - I_A^*)^2 \\
& + \frac{\gamma}{I_A}(E I_A^* + E^* I_A) + \frac{c_6}{I_S}(I_S - I_S^*)^2 + \frac{\delta_1}{I_S}(I_A I_S^* + I_A^* I_S)]. \qquad (34)
\end{aligned}
$$

and with $P > 0$ and $Q > 0$. Thus $L^{\cdot} = P - Q < 0$ iff $P < Q$ and $L^{\cdot} = 0$ if and only if $S_i = S_i^*$, $E = E^*$, $I_A = I_A^*$, $I_S = I_S^*$ for $i = 0, 1, 2, 3$. The EE point P_1 exists if and only if $R_0 > 1$, and the singleton set $\{P_1\}$ is the biggest compact invariant set in $\{(S_0, S_1, S_2, S_3, E, I_A, I_S) \in \Delta : \frac{dL}{dt} = 0\}$. According to LaSalle's invariance principle [56], the EE point $\{P_1\}$ is GAS in Δ if $P < Q$. □

6. Bifurcation analysis

The Castilla-Chavez and Song [33] approach is used to study the bifurcation nature of system (1).

Theorem 8. *The system (1) has forward bifurcation at $\beta_1 = \beta_1^*$ (i.e. at $R_0 = 1$) whenever $a < 0$, where expression for β_1^* and a are given in the proof.*

Proof. Let $S_i = x_{i+1}$ for $i = 0, 1, 2, 3$, $E = x_5$, $I_A = x_6$, $I_S = x_7$. The transformed system becomes

$$
\begin{aligned}
x_1^{\cdot} &= \Lambda - \beta_1 x_1 x_6 - c_1 x_1 . \\
x_2^{\cdot} &= \alpha_1 x_1 - \beta_2 x_2 x_6 - c_2 x_2 . \\
x_3^{\cdot} &= \alpha_2 x_2 - \beta_3 x_3 x_6 - c_3 x_3 . \\
x_4^{\cdot} &= \alpha_3 x_3 - \xi x_4 . \\
x_5^{\cdot} &= (\beta_1 x_1 + \beta_2 x_2 + \beta_3 x_3) x_6 - c_4 x_5 . \\
x_6^{\cdot} &= \gamma x_5 - c_5 x_6 . \\
x_7^{\cdot} &= \delta_1 x_6 - c_6 x_7 .
\end{aligned} \qquad (35)
$$

where $c_1 = \alpha_1 + \xi$ $c_2 = \alpha_2 + \xi$, $c_3 = \alpha_3 + \xi$, $c_4 = \gamma + \xi$, $c_5 = \delta_1 + \delta_2 + \xi$, $c_6 = \sigma_1 + \sigma_2 + \xi$. The transmission rate of the non-vaccinated susceptible population is considered as the bifurcation parameter with the restriction $R_0 = 1$. Hence we get

$$
\beta_1^* = \frac{c_1 c_2 c_3 c_4 c_5 - \gamma \Lambda c_3 \alpha_1 \beta_2 - \gamma \Lambda \alpha_1 \alpha_2 \beta_3}{\gamma \Lambda c_2 c_3}. \qquad (36)
$$

The transformed system has the disease free equilibrium point $P_0 = (x_1^0, x_2^0, x_3^0, x_4^0, x_5^0, x_6^0, x_7^0)$, where $x_1^0 = \frac{\Lambda}{c_1}$, $x_2^0 = \frac{\Lambda \alpha_1}{c_1 c_2}$, $x_3^0 = \frac{\Lambda \alpha_1 \alpha_2}{c_1 c_2 c_3}$, $x_4^0 = \frac{\Lambda \alpha_1 \alpha_2 \alpha_3}{\xi c_1 c_2 c_3}$, $x_5^0 = 0$, $x_6^0 = 0$, $x_7^0 = 0$. $J(P_0)$, provided in Eq. (13), is the linearisation matrix of the transformed system at P_0. At $\beta_1 = \beta_1^*(R_0 = 1)$, the jacobian of system (35) has one zero eigenvalue, while the other eigenvalues have a negative real part. As a result, the dynamics of the transformed system near $\beta_1 = \beta_1^*(R_0 = 1)$ are studied using the central manifold theory [33]. The necessary calculations as per the central manifold theory [33] is as follows. $W = (w_1, w_2, w_3, w_4, w_5, w_6, w_7)^T$ is the right eigenvector for $J(P_0)$ when $R_0 = 1$ is computed using $J(P_0) \cdot W = 0$ and hence

$$
w_1 = \frac{\gamma \Lambda (c_3 \alpha_1 \beta_2 + \alpha_1 \alpha_2 \beta_3) - c_1 c_2 c_3 c_4 c_5}{c_1^2 c_2 c_3 c_5} w_5, \quad w_2 = -\frac{\alpha_1 (c_1 c_2 c_3 c_4 c_5 + \gamma \Lambda (c_1 c_3 \beta_2 + c_3 \alpha_1 \beta_2 + \alpha_1 \alpha_2 \beta_3))}{c_1^2 c_2^2 c_3 c_5} w_5,
$$

$$
w_3 = -\frac{\alpha_1 \alpha_2 (c_1 c_2 c_3 c_4 c_5 + \gamma \Lambda (c_1 c_3 \beta_2 + c_3 \alpha_1 \beta_2 + c_1 c_2 \beta_3 + \alpha_1 \alpha_2 \beta_3))}{c_1^2 c_2^2 c_3^2 c_5} w_5, \quad w_6 = \frac{\gamma}{c_5} w_5, \quad w_7 = \frac{\gamma \delta_1}{c_5 c_6} w_5
$$

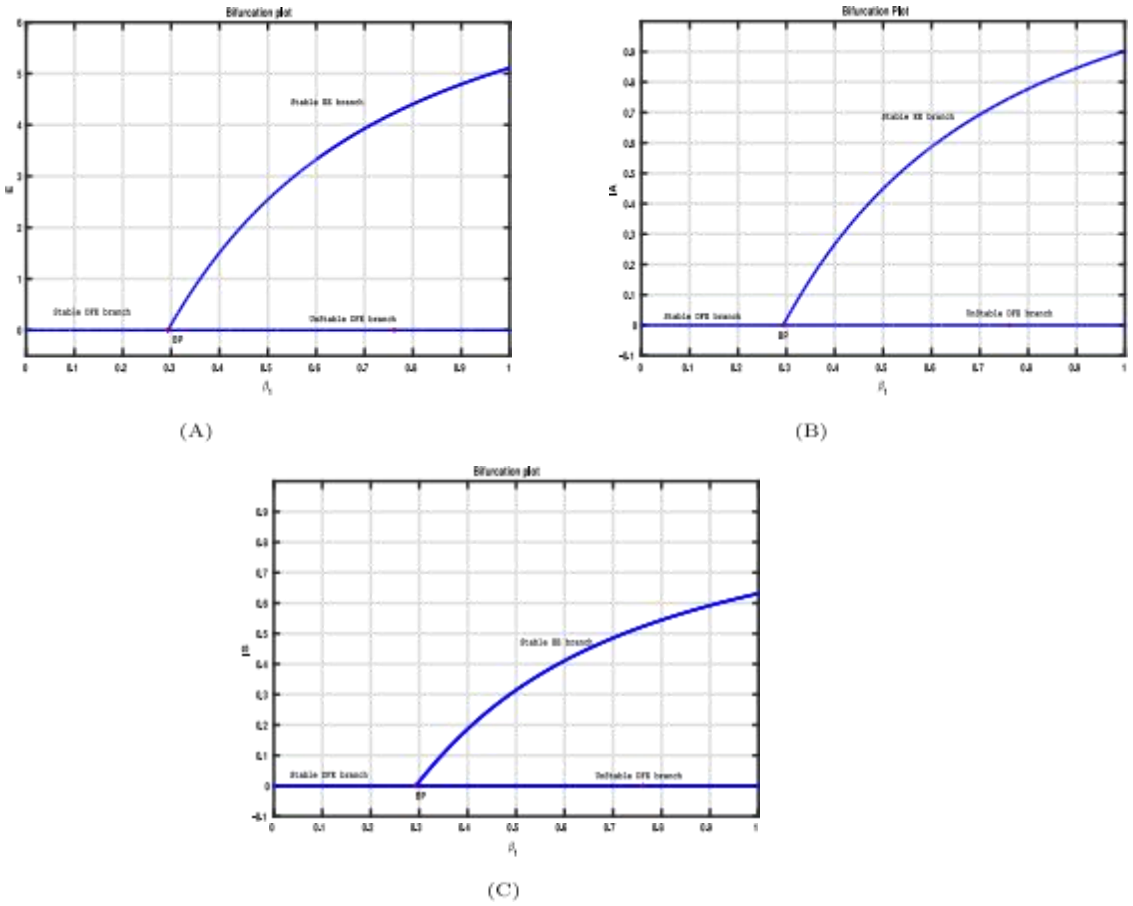

Fig. 2. Bifurcation plot showing the bifurcation point $\beta_1^*(R_0 = 1) = 0.29325$ at which the forward bifurcation occurs with parameters values from the Table 5.

$$w_4 = -\frac{\alpha_1\alpha_2\alpha_3(c_1c_2c_3c_4c_5 + \gamma\Lambda(c_1c_3\beta_2 + c_3\alpha_1\beta_2 + c_1c_2\beta_3 + \alpha_1\alpha_2\beta_3))}{\xi c_1^2c_2^2c_3^2c_5}w_5.$$

$V=(v_1, v_2, v_3, v_4, v_5, v_6, v_7)$ is the left eigenvector of jacobian matrix $J(P_0)$ when $R_0 = 1$ is computed using $V.J(P_0) = 0$ and hence we get, $v_i = 0$ for $i = 1, 2, 3, 4, 7$, $v_6 = \frac{c_4}{\gamma}v_5$. Then, v_5 is calculated to ensure that condition $V.W = 1$ is met and hence $v_5 = \frac{c_5}{(c_4+c_5)w_5}$ and $v_6 = \frac{c_4c_5}{\gamma(c_4+c_5)w_5}$. The bifurcation coefficients are given by

$$\begin{aligned} a &= \sum_{k,i,j=1}^{7} v_k w_i w_j \frac{\partial^2 f_k(P_0, \beta_1^*)}{\partial x_i \partial x_j}. \\ b &= \sum_{k,i,j=1}^{7} v_k w_i \frac{\partial^2 f_k(P_0, \beta_1^*)}{\partial x_i \partial \beta_1}. \end{aligned} \tag{37}$$

The following expressions give the bifurcation coefficients a and b after simplification

$$a = \frac{2w_5(\gamma\Lambda c_2c_3^2c_4c_5\alpha_1\beta_2 + \gamma\Lambda c_2c_3c_4c_5\alpha_1\alpha_2\beta_3 - \gamma^2\Lambda^2c_3\alpha_1\alpha_2\beta_2\beta_3 - \gamma^2\Lambda^2c_2\alpha_1\alpha_2\beta_3^2 - c_1c_2^2c_3^2c_4^2c_5^2 - \gamma^2\Lambda^2c_3^2\alpha_1\beta_2^2)}{\Lambda c_1c_2^2c_3^2c_5(c_4 + c_5)}. \tag{38}$$

$$b = \frac{\gamma\Lambda}{c_1(c_4 + c_5)} > 0. \tag{39}$$

As a result, when $a < 0$, the system (1) at $R_0 = 1$ experiences forward bifurcation. In forward bifurcation, when $R_0 > 1$, an unstable disease-free equilibrium coexists with a stable endemic equilibrium point. □

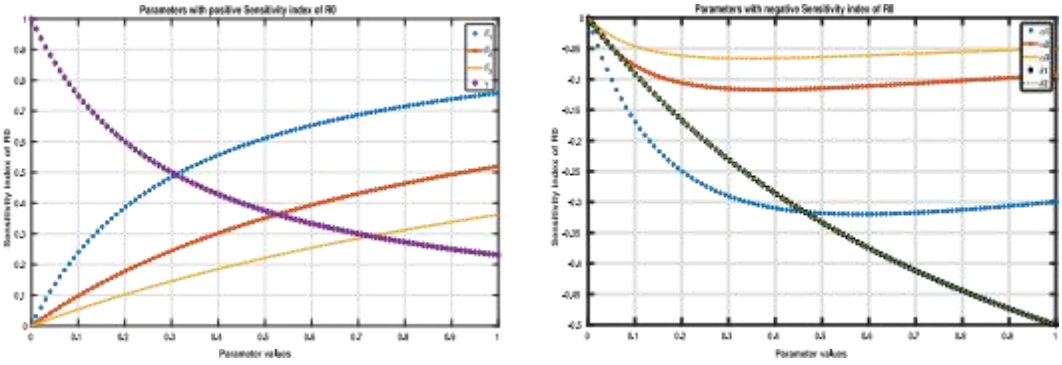

(A) (B)

Fig. 3. Sensitivity index plot of (A) The parameters with positive sensitivity index, and (B) The parameters with negative sensitivity index.

7. Analysis of sensitivity

A sensitivity study was performed on the system (1) to see how different factors affected OMICRON variant disease transmission in the Indian population. The parameters that have a substantial impact on the system (1)'s BRN are highlighted in this analysis. The health authorities can better manage the spread of the disease by analysing the parameters in relation to the BRN. Sensitivity analysis helps with experiment design, data assimilation, and reduction of complex non-linear models. The normalised forward sensitivity indexof R_0 that depends differentiably on a parameter $m$is defined as $\Gamma_m^{R_0} = \frac{\partial R_0}{\partial m}\frac{m}{R_0}$. Here $R_0 = \frac{\gamma\Lambda(\beta_1 c_2 c_3 + \beta_2\alpha_1 c_3 + \beta_3\alpha_1\alpha_2)}{c_1 c_2 c_3 c_4 c_5}$, where $c_1 = \alpha_1 + \xi$, $c_2 = \alpha_2 + \xi$, $c_3 = \alpha_3 + \xi$, $c_4 = \gamma + \xi$, $c_5 = \delta_1 + \delta_2 + \xi$. Then the sensitivity index of R_0 that depends on various parameters of the system (1) is given as follows. $\Gamma_\Lambda^{R_0} = 1 > 0$, $\Gamma_{\beta_1}^{R_0} = \frac{0.64\beta_1}{0.204+0.64\beta_1} > 0$, $\Gamma_{\beta 2}^{R_0} = \frac{0.48\beta_2}{0.444+0.48\beta_2} > 0$, $\Gamma_{\beta 3}^{R_0} = \frac{0.3\beta_3}{0.528+0.3\beta_3} > 0$, $\Gamma_\xi^{R_0} = -\frac{\xi(0.4482+\xi(3.3856+\xi(9.869+\xi(14.21+(10.3+3\xi)\xi))))}{0.063+\xi(0.6498+\xi(2.6846+\xi(5.739+\xi(6.73+\xi(4.1+\xi)))))} < 0$, $\Gamma_\gamma^{R_0} = \frac{0.3+2.46515\times10^{-16}\gamma}{0.3+\gamma} > 0$, $\Gamma_{\delta 1}^{R_0} = -\frac{\delta_1}{1+\delta_1} < 0$, $\Gamma_{\delta 2}^{R_0} = -\frac{\delta_2}{1+\delta_2} < 0$, $\Gamma_{\alpha_1}^{R_0} = -\frac{(0.829412+3.55271\times10^{-16}\alpha_1)\alpha_1}{(0.3+\alpha_1)(1.12941+\alpha_1)} < 0$, $\Gamma_{\alpha 2}^{R_0} = -\frac{(0.18+1.5099\times10^{-16}\alpha_2)\alpha_2}{(0.3+\alpha_2)(0.48+\alpha_2)} < 0$, $\Gamma_{\alpha 3}^{R_0} = -\frac{(0.0909091+2.74528\times10^{-16}\alpha_3)\alpha_3}{(0.3+\alpha_3)(0.390909+\alpha_3)} < 0$.

From Fig. 4(B), the sensitivity indexof β_2, say $\Gamma_{\beta 2}^{R_0} = \Gamma_{\beta 2}^{R_0} = \frac{0.48\beta_2}{0.444+0.48\beta_2}$ is approximately 0.3 for $\beta_2 = 0.4$. The physical meaning of this positive sensitivity indexof β_2 is that increasing (or decreasing) β_2 by 10% increases (or decreases) R_0 value by 3%. From Fig. 4(J), the sensitivity indexof α_3, say $\Gamma_{\alpha 3}^{R_0} = -\frac{(0.0909091+2.74528\times10^{-16}\alpha_3)\alpha_3}{(0.3+\alpha_3)(0.390909+\alpha_3)}$ is approximately -0.06 for $\alpha_3 = 0.6$. The physical meaning of this negative sensitivity indexof α_3 is that increasing (or decreasing) α_3 by 10% decreases (or increases) R_0 value by 0.6%. A highly sensitive parameter must be carefully estimated, as a very small variation in that parameter will result to large quantitative changes to the system (1).

From Fig. 3(A), it is evident that the parameter with the most positive sensitivity index relative to R_0 is β_1, the infection transmission rate among the non-vaccinated susceptible population. The remaining parameters with positive sensitivity are β_2,β_3 and γ arranged from most sensitive to least sensitive positive index.

From the Fig. 3(B), it is seen that the most sensitive parameter among the parameters with a negative sensitivity index is δ_1, the proportion of the asymptomatic infected population who develop symptoms of the disease and δ_2, the recovery rate of asymptomatic infected individuals. The remaining parameters with negative sensitivity are α_1, α_2 and α_3 arranged from most sensitive to least sensitive negative index.

By examining R_0's sensitivity indices in relation to various parameters, it is reasonable to conclude that disease transmission rates β_1, β_2 and β_3 with positive sensitivity indices should be minimised to keep the disease from spreading. Furthermore, vaccination administration rates, specifically α_1, α_2 and α_3 with a negative sensitivity index, should be maximised to prevent the spread of the disease in society.

Solution trajectories for the infected populations, namely I_A and I_S, are plotted for distinct values of parameters with the same preliminary conditions to identify the sensitive parameters of the system (1). The parameters in the Table 1 with preliminary conditions $S_0(0) = 10$, $S_1(0) = 9$, $S_2(0) = 8$, $S_3(0) = 7$, $E(0) = 6$, $I_A(0) = 5$, $I_S(0) = 4$ are used to numerically simulate system (1). For different values of the disease transmission rate, say $\beta_1 = 0.3, 0.5$

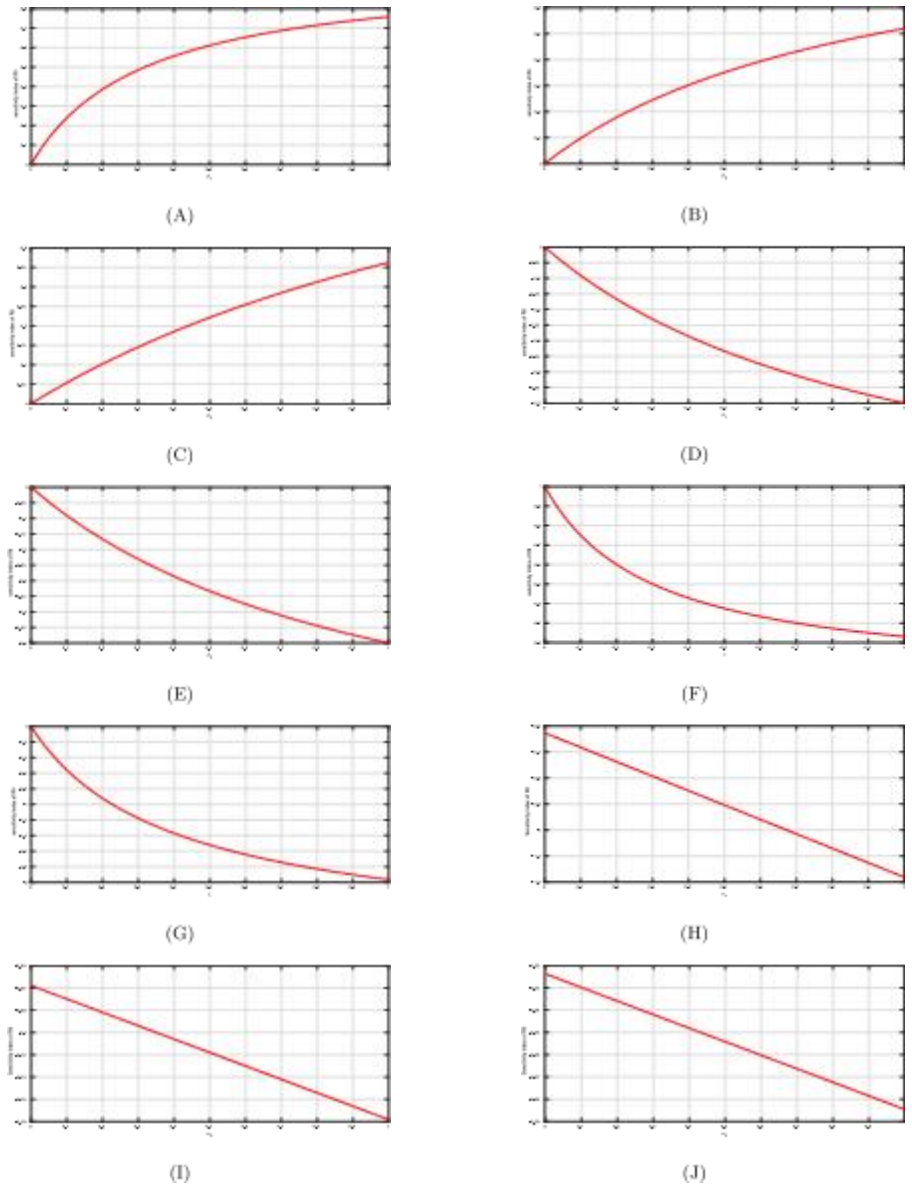

Fig. 4. The plot of the sensitivity indices of R_0 depends on (A) The disease transmission rate of non-vaccinated susceptible population β_1, (B) The disease transmission rate of dose-1 vaccinated susceptible population β_2, (C) The disease transmission rate of dose-2 vaccinated susceptible population β_3, (D) δ_1, the proportion of infected but asymptomatic individuals exposing symptoms, (E) The recovery rate of asymptomatic infected individuals from the disease δ_2, (F) The rate of exposed individuals who are asymptomatic to the disease γ, (G) ξ, each population's natural death rate, (H) The dose-1 vaccination rate α_1 administered to non-vaccinated susceptible population, (I) The dose-2 vaccination rate α_2 administered to dose-1 vaccinated susceptible population, (J) The booster dose vaccination rate α_3 administered to dose-2 vaccinated susceptible population.

and 0.7 of the non-vaccinated susceptible population, S_0, the time series of infected human populations are plotted in Figs. 5(A) and 5(B), respectively. The figures clearly show that the number of infected cases in both populations increased as β_1 levels increased. As a result, the disease transmission rate β_1 among the non-vaccinated susceptible population is crucial to the disease's spread.

Figs. 6(A) and 6(B) show time series of asymptomatic infected and symptomatic infected human populations for different values of the disease transmission rate among the dose-1 vaccinated susceptible population S_1, such as

Table 1
Description of the model parameters.

Parameter	Description
Λ	The non-vaccinated susceptible population's recruitment rate.
β_1	Non-vaccinated susceptible population's infection transmission rate.
β_2	Disease transmission rate of dose-1 vaccinated susceptible population.
β_3	The disease transmission rate of dose-2 vaccinated susceptible population.
α_1	The rate of dose-1 vaccination given to non-vaccinated individuals.
α_2	The rate of dose-2 vaccination given to dose-1 vaccinated individuals.
α_3	The rate of booster dose vaccination given to dose-2 vaccinated individuals.
ξ	The proportion of death in all populations.
γ	The proportion of the exposed population who are infected without symptoms.
δ_1	The proportion of the asymptomatic infected population who develop symptoms of the disease.
δ_2	The recovery rate of asymptomatic infected individuals.
σ_1	The recovery rate of symptomatic infected individuals.
σ_2	The disease-induced death rate of symptomatic infected individuals.

Table 2
Sensitivity values of R_0.

Parameters	Λ	β_1	β_2	β_3	α_1	α_2	α_3	ξ	γ	δ_1	δ_2
Sign of sensitivity index of R_0	+	+	+	+	–	–	–	–	+	–	–

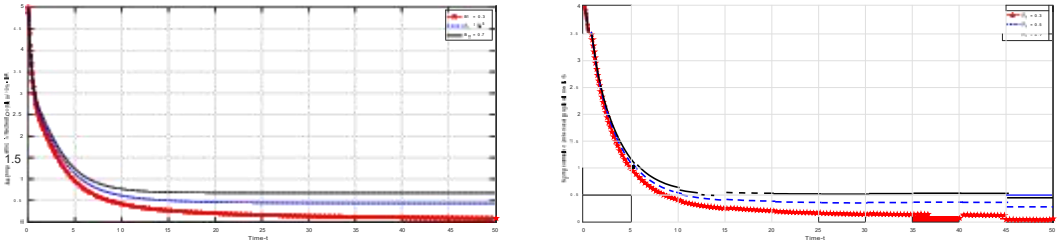

(A) (B)

Fig. 5. A plot of the infected populations I_A and I_S over time for $\beta_1 = 0.3, 0.5, 0.7$.

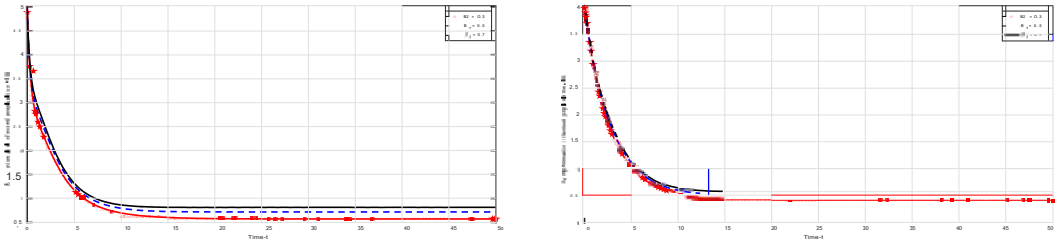

(A) (B)

Fig. 6. A plot of the infected populations I_A and I_S over time for $\beta_2 = 0.3, 0.5, 0.7$.

$\beta_2 = 0.3$, 0.5, and 0.7. The increase in β_2 increases the number of infected cases in both populations, as seen in the figures. As a result, the disease transmission rate β_2 within the dose-1 vaccinated susceptible group S_1 is critical to the disease's spread.

Figs. 7(A) and 7(B) show time series of asymptomatic infected and symptomatic infected human populations for different values of the disease transmission rate among the dose-2 vaccinated susceptible population S_2, i.e., $\beta_3 = 0.3$, 0.5, and 0.7. The figure shows that the total infected cases in the I_A and I_S populations do not

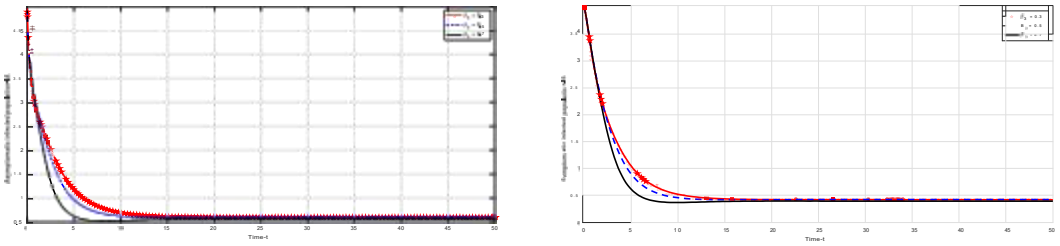

(A) (B)

Fig. 7. A plot of the infected populations I_A and I_S over time for $\beta_3 = 0.3, 0.5, 0.7$.

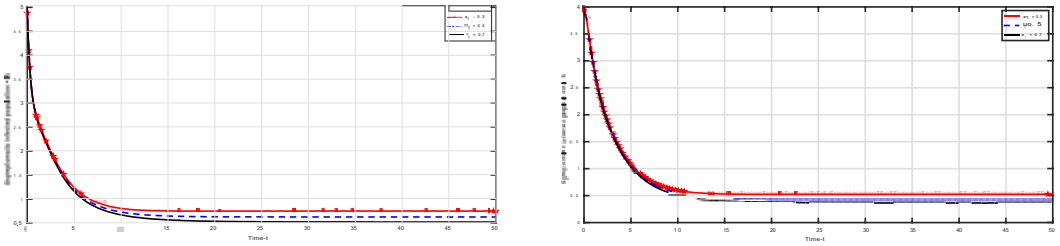

(A) (B)

Fig. 8. A plot of the infected populations I_A and I_S over time for $\alpha_1 = 0.3, 0.5, 0.7$.

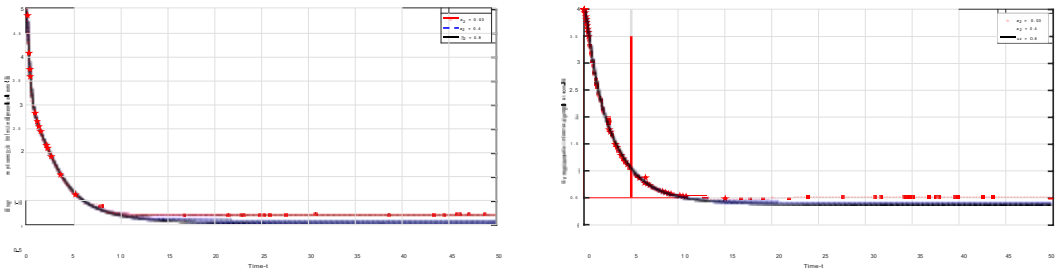

(A) (B)

Fig. 9. A plot of the infected populations I_A and I_S over time for $\alpha_2 = 0.3, 0.5, 0.7$.

change much when β_3 increases. As a result, the disease does not spread rapidly among the susceptible population who have received both vaccine doses. This emphasises the importance of administering two doses to a susceptible population.

Figs. 8(A) and 8(B) show time series of asymptomatic infected and symptomatic infected human populations for different values of the dose-1 vaccination rate among the non-vaccinated susceptible population S_0, such as $\alpha_1 = 0.3, 0.5$, and 0.7. The figures clearly show that when the dose-1 vaccination rate rises, the number of infected individuals in both populations drops. As a result, the dose-1 vaccination rate among the non-vaccinated susceptible population S_0 is critical in limiting disease spread.

Figs. 9(A) and 9(B) show time series of asymptomatic and symptomatic infected human populations for distinct values of the dose-2 vaccination rate within the dose-1 vaccinated susceptible population S_1, such as $\alpha_2 = 0.3, 0.5$, and 0.7. The rise in the dose-2 vaccination rate α_2 reduces the number of infected cases in both populations, as seen in the figures. As a result, the dose-2 vaccination rate among the dose-1 vaccinated susceptible population S_1 is critical in limiting disease spread.

Figs. 10(A) and 10(B) show time series of asymptomatic and symptomatic infected human populations for various values of the booster dose vaccination rate among the dose-2 vaccinated susceptible population S_2, such

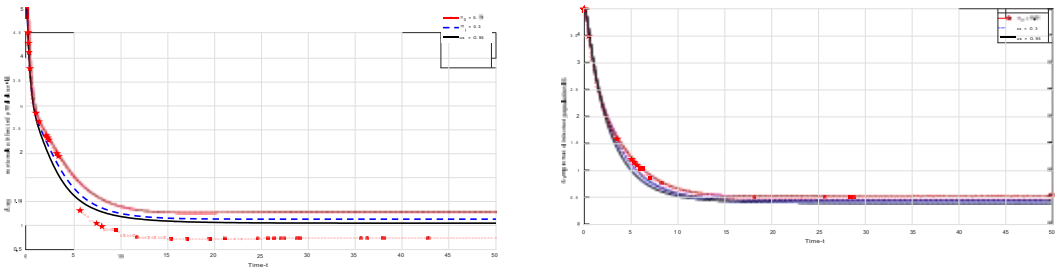

(A) (B)

Fig. 10. A plot of the infected populations I_A and I_S over time for $\alpha_3 = 0.01, 0.3, 0.95$.

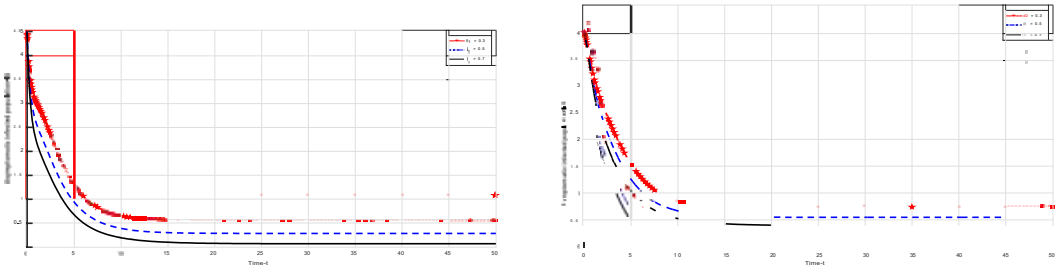

(A) (B)

Fig. 11. A plot of the infected populations I_A and I_S over time for $\delta_1 = 0.3, 0.5, 0.7$ and $\delta_2 = 0.3, 0.5, 0.7$ respectively.

as $\alpha_3 = 0.01$, 0.3, and 0.95. It is apparent from these data that are increasing the booster dose vaccination rate α_3 in the dose-2 vaccinated susceptible population S_2 reduces the number of infected cases in both the populations I_A and I_S. These results demonstrate the relevance of delivering the booster dose vaccine in addition to the dose-2 vaccination among S_2.

Figs. 11(A) and 11(B) show the time series of asymptomatic infected and symptomatic infected human populations for various values of the parameters, $\delta_1 = 0.3$, 0.5, 0.7 and $\delta_2 = 0.3$, 0.5, 0.7, respectively. The asymptomatic infected population I_A drops steadily whenever the rate of infected individuals showing signs of the disease δ_1 increases, as shown in Fig. 11(A), and hence, disease spread is minimised. Fig. 11(A) emphasises the need to employ suitable testing methods to detect asymptomatic infected persons. The symptomatic infected population I_S is steadily reduced as the rate of infected persons without symptoms recovered from the disease δ_2 increases, as shown in Fig. 11(B).

8. Parameter estimation

The following values of parameters are used to analyse the effect of the OMICRON variant virus in India using our proposed mathematical model. The following approach is employed to estimate some parameter values and the preliminary values of eight populations. According to the most recent WHO data published in 2018 [10], males have a life expectancy of 67.4 years, and females have a life expectancy of 70.3 years, for a total life expectancy of 68.8 years. As a result, each population's natural mortality rate ξ is estimated to be $\frac{1}{365\times 68.8} = 0.00004$ deaths per day. According to UNICEF [11], there are approximately 70000 births per day in India. Therefore the recruitment rate Λ is assumed as 70,000 births per day. The values of the parameters α_1, α_2, and α_3 are determined based on the vaccination administration speed, whereas β_1, β_2, and β_3 are chosen hypothetically and adjusted using the least square approach to fit our model with accurate data. The incubation period for COVID-19 disease caused by the Omicron variant virus is 2 to 4 days [12]. As a result, we assume that our model's incubation time is three days, resulting in the value of the $\gamma = \frac{1}{3} = 0.33$ exposed individuals infected every day. Patients with COVID-19 caused by an omicron variant usually recover after five days [13]. As a result, δ_2 is considered $\frac{1}{5} = 0.2$ infected persons recovering per day. To fit our model with actual data, the parameters δ_1, σ_1, and σ_2 are set hypothetically and changed using the least square approach.

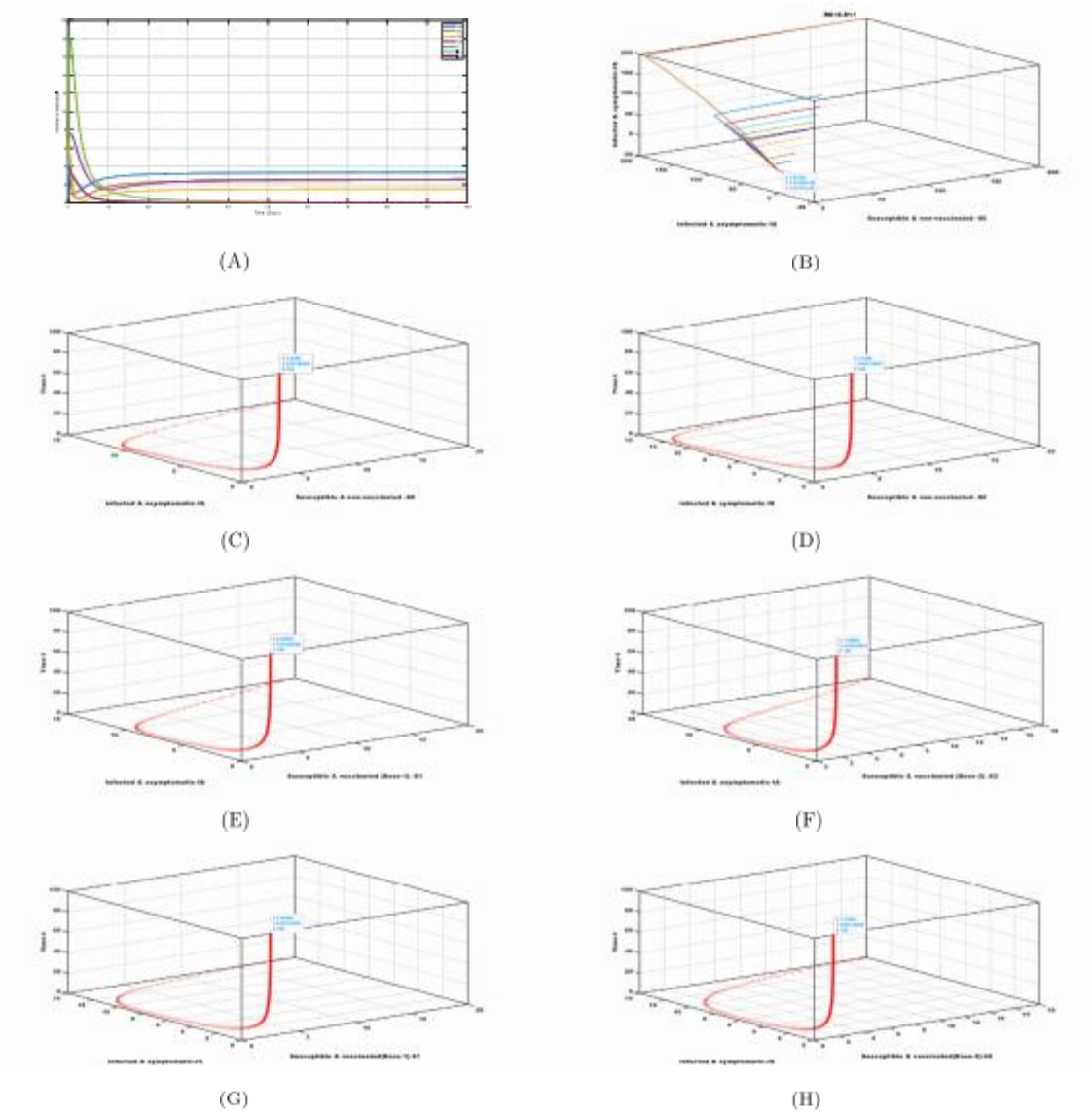

Fig. 12. (A) The local stability of P_0 of the omicron model (1) for $R_0 < 1$, (B) Global stability of disease free equilibrium shown in $S_0 - I_A - I_S$ phase space for $R_0 < 1$, (C) Susceptible population without vaccination (S_0) against infected & asymptomatic population (I_A) over time 't' for $R_0 < 1$, (D) Susceptible population without vaccination (S_0) against infected & symptomatic population (I_S) over time 't' for $R_0 < 1$, (E) Susceptible population & vaccinated with dose-1 (S_1) against infected & asymptomatic population (I_A) over time 't' for $R_0 < 1$, (F) Susceptible population & vaccinated with dose-2 (S_2) against infected & asymptomatic population (I_A) over time 't' for $R_0 < 1$, (G) Susceptible population & vaccinated with dose-1 (S_1) against infected & symptomatic population (I_S) over time 't' for $R_0 < 1$ and (H) Susceptible population & vaccinated with dose-2 (S_2) against infected & symptomatic population (I_S) over time 't' for $R_0 < 1$.

9. Numerical analysis

This section carried out simulation tests to verify the analytically derived results. The proposed OMICRON model (1) has been subjected to simulations portraying local and global stability. The parameter values are taken from the Tables 4 and 5, respectively, for $R_0 < 1$ and $R_0 > 1$.

The DFE point $P_0(S_0^0, S_1^0, S_2^0, S_3^0, E^0, I_A^0, I_S^0)$'s global and local stability has been numerically simulated and depicted in Fig. 12. The disease free equilibrium is found to be $P_0(3.33, 2.5, 1.5625, 2.60417, 0, 0, 0)$ and $R_0 = 0.9 < 1$ using the parameter values from Table 4. Hence for various initial conditions on the state variables

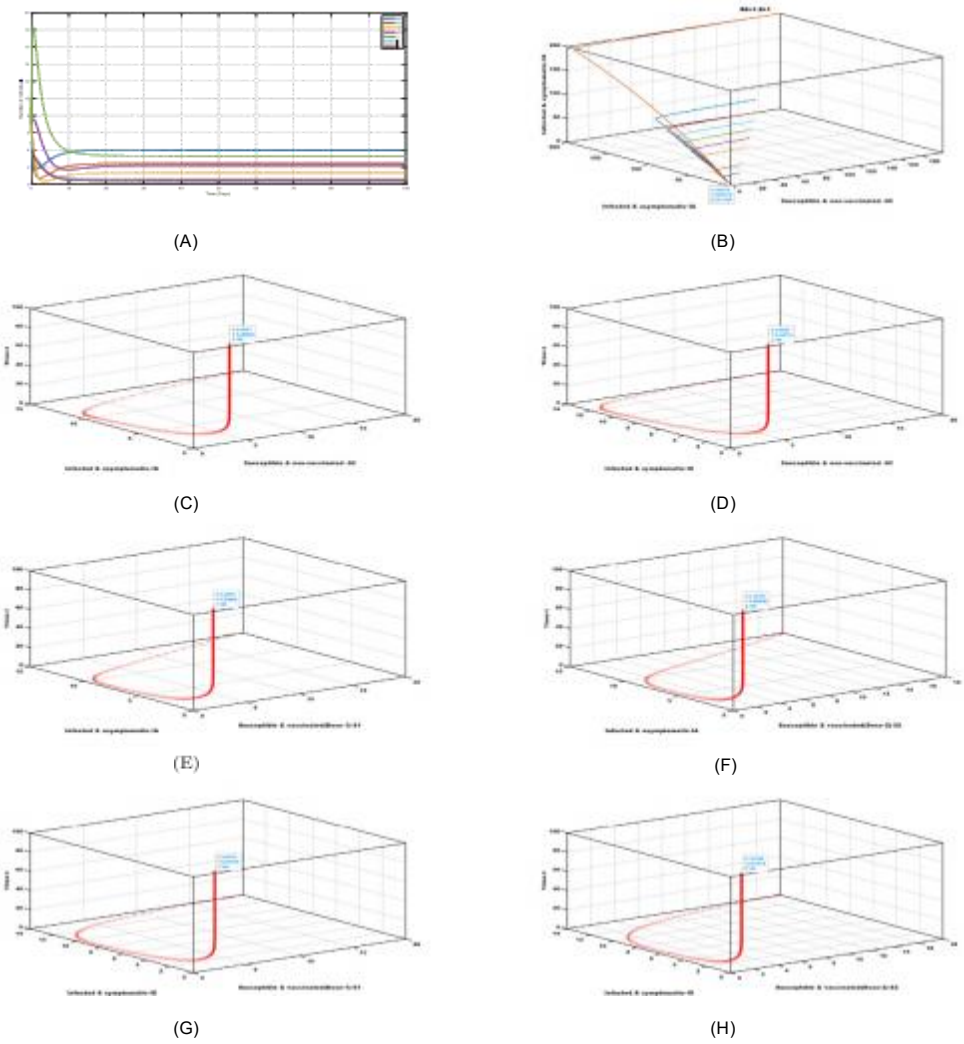

Fig. 13. (A) The LAS of P_1 of the omicron system (1) for $R_0 > 1$, (B) GAS of P_1 shown in $S_0 - I_A - I_S$ phase plane for $R_0 > 1$, (C) Susceptible population without vaccination (S_0) against infected & asymptomatic population (I_A) over time 't' for $R_0 > 1$, (D) Susceptible population without vaccination (S_0) against infected & symptomatic population (I_S) over time 't' for $R_0 > 1$, (E) Susceptible population & vaccinated with dose-1 (S_1) against infected & asymptomatic population (I_A) over time 't' for $R_0 > 1$, (F) Susceptible population & vaccinated with dose-2 (S_2) against infected & asymptomatic population (I_A), (G) Susceptible population & vaccinated with dose-1 (S_1) against infected & symptomatic population (I_S) over time 't' for $R_0 > 1$ and (H) Susceptible population & vaccinated with dose-2 (S_2) against infected & symptomatic population (I_S) over time 't' for $R_0 > 1$.

near the equilibrium point P_0, it is seen from the Fig. 12(A) that $\lim_{t\to\infty} S_0(t) = S_0^0 = 3.33$, $\lim_{t\to\infty} S_1(t) = S_1^0 = 2.5$, $\lim_{t\to\infty} S_2(t) = S_2^0 = 1.5625$, $\lim_{t\to\infty} S_3(t) = S_3^0 = 2.60417$, $\lim_{t\to\infty} E(t) = E^0 = 0$, $\lim_{t\to\infty} I_A(t) = I_A^0 = 0$ and $\lim_{t\to\infty} I_S(t) = I_S^0 = 0$. From Fig. 12(C), it is seen that the populations $S_0(t)$ and $I_A(t)$ converge to $S_0^0 = 3.3$ and $I_A^0 = 0$ respectively as $t \to \infty$ for initial points of state variables near P_0. Similarly from Figs. 12(D), 12(E), 12(F), 12(G) and 12(H), it is seen that the state variables $(S_0(t), I_S(t)) \to (S_0^0, I_S^0) = (3.33, 0)$, $(S_1(t), I_A(t)) \to (S_1^0, I_A^0) = (2.5, 0)$, $(S_2(t), I_A(t)) \to (S_2^0, I_A^0) = (1.5625, 0)$, $(S_1(t), I_S(t)) \to (S_1^0, I_S^0) = (2.5, 0)$ and $(S_2(t), I_S(t)) \to (S_2^0, I_S^0) = (1.5625, 0)$ as $t \to \infty$ respectively whenever the initial populations are chosen near P_0. As stated in Theorem 3, the local stability of P_0 whenever $R_0 < 1$ is verified. From figure Fig. 12(B), it is noticed that for any initial conditions on the state variables $S_0(t)$, $I_A(t)$ and $I_S(t)$ in Δ_1, the solution trajectories $(S_0(t), I_A(t), I_S(t)) \to$

Table 3
Parameter values with assumed and real field values used in constructing the Figs. 14–17.

Parameters	Values	Source
Λ	70000	[11]
α_1	0.0085	assumed
α_2	0.012	assumed
α_3	0.0001	assumed
β_1	2×10^{-10}	assumed
β_2	2×10^{-10}	assumed
β_3	1×10^{-9}	assumed
γ	0.33	[12]
δ_1	0.0012	assumed
δ_2	0.2	[13]
σ_1	0.1	assumed
σ_2	0.00001	assumed
ξ	0.00004	[10]

Table 4
Parameter values for constructing Fig. 12.

Parameters	Λ	β_1	β_2	β_3	α_1	α_2	α_3	ξ	γ	δ_1	δ_2	σ_1	σ_2
Values	3	0.6	0.3	0.2	0.6	0.5	0.5	0.3	0.3	0.7	0.7	0.3	0.4

Table 5
Parameter values for constructing Fig. 13.

Parameters	Λ	β_1	β_2	β_3	α_1	α_2	α_3	ξ	γ	δ_1	δ_2	σ_1	σ_2
Values	5	0.6	0.3	0.2	0.6	0.5	0.5	0.3	0.3	0.7	0.7	0.3	0.4

$(S_0^0, I_A^0, I_S^0) = (3.33, 0, 0)$ as $t \to \infty$. This convergence can be verified for all possible ordered triples out of the seven state variables. As stated in Theorem 5, P_0 is GAS in Δ_1 whenever $R_0 < 1$ is verified.

The global and local stability of the endemic equilibrium $P_1(S_0^*, S_1^*, S_2^*, S_3^*, E^*, I_A^*, I_S^*)$ has been numerically simulated and portrayed in the Fig. 13. The endemic equilibrium point is found to be $P_1(3.9933, 2.45477, 1.33795, 2.229917, 3.32537, 0.58683, 0.410781)$ and $R_0 = 1.5 > 1$ using the parameter values from Table 5. Hence for various initial conditions on the state variables near the equilibrium point P_1, it is seen from the Fig. 13(A) that $\lim_{t\to\infty} S_0(t) = S_0^* = 3.9933$, $\lim_{t\to\infty} S_1(t) = S_1^* = 2.45477$, $\lim_{t\to\infty} S_2(t) = S_2^* = 1.33795$, $\lim_{t\to\infty} S_3(t) = S_3^* = 2.229917$, $\lim_{t\to\infty} E(t) = E^* = 3.32537$, $\lim_{t\to\infty} I_A(t) = I_A^* = 0.58683$ and $\lim_{t\to\infty} I_S(t) = I_S^* = 0.410781$. From Fig. 13(C), it is seen that the populations $S_0(t)$ and $I_A(t)$ converges to $S_0^* = 3.9933$ and $I_A^* = 0.58683$ respectively as $t \to \infty$ for initial points of state variable near P_1. Similarly from the Figs. 13(D), 13(E), 13(F), 13(G) and 13(H) it is seen that the state variables $(S_0(t), I_S(t)) \to (S_0^*, I_S^*) = (3.9933, 0.410781)$, $(S_1(t), I_A(t)) \to (S_1^*, I_A^*) = (2.45477, 0.58683)$, $(S_2(t), I_A(t)) \to (S_2^*, I_A^*) = (1.33795, 0.58683)$, $(S_1(t), I_S(t)) \to (S_1^*, I_S^*) = (2.45477, 0.410781)$ and $(S_2(t), I_S(t)) \to (S_2^*, I_S^*) = (1.33795, 0.410781)$ as $t \to \infty$ respectively whenever the initial populations are chosen near P_1. Further the necessary and sufficient conditions stated in the Theorem 6, say $|H_1| = B_1 = 5.44551 > 0$, $|H_2| = 48.2477 > 0$, $|H_3| = 336.786 > 0$, $|H_4| = 902.45 > 0$ and $|H_5| = 355.561 > 0$ with $B_1 = 5.44551 > 0$, $B_2 = 10.5008 > 0$, $B_3 = 8.93463 > 0$, $B_4 = 3.25204 > 0$, $B_5 = 0.393995 > 0$, are satisfied. As stated in Theorem 6, the LAS of the point P_1 is verified whenever $R_0 > 1$. From Fig. 13(B), it is noticed that for any initial conditions on the state variables $S_0(t)$, $I_A(t)$ and $I_S(t)$ in Δ, the solution trajectories $(S_0(t), I_A(t), I_S(t)) \to (S_0^*, I_A^*, I_S^*) = (3.9933, 0.58683, 0.410781)$ as $t \to \infty$. This convergence can be verified for all possible ordered triples out of the seven state variables. As stated in Theorem 7, it is verified that P_1 is GAS in Δ when $R_0 > 1$.

According to WHO data as of December 28th, 2021, the initial susceptible vaccination populations of dose-1 and dose-2 and active OMICRON-infected populations are assumed to be $S_1 = 254121172$, $S_2 = 585974301$, $I_S = 80621$, respectively. The remaining initial populations are hypothetically chosen for numerical simulation as

Table 6
Real confirmed COVID-19 infected cases in the Indian population.

Date	29-12-2021	30-12-2021	31-12-2021	1-1-2022	2-1-2022	3-1-2022
Active cases	86158	95214	109995	130000	152690	179098
Date	4-1-2022	5-1-2022	6-1-2022	7-1-2022	8-1-2022	9-1-2022
Active cases	210261	280409	300000	468419	586858	720580
Date	10-1-2022	11-1-2022	12-1-2022	13-1-2022	14-1-2022	15-1-2022
Active cases	835000	951560	1113769	1268309	1414025	1500000
Date	16-1-2022	17-1-2022	18-1-2022	19-1-2022	20-1-2022	21-1-2022
Active cases	1652538	1732831	1827199	1920244	2000000	2109548
Date	22-1-2022	23-1-2022	24-1-2022	25-1-2022	26-1-2022	27-1-2022
Active cases	2183398	2245489	2233040	2200000	2198632	2101766
Date	28-1-2022	29-1-2022	30-1-2022	31-1-2022	1-2-2022	2-2-2022
Active cases	2000490	1881088	1800000	1739187	1617723	1530050
Date	3-2-2022	4-2-2022	5-2-2022	6-2-2022	7-2-2022	8-2-2022
Active cases	1400000	1327735	1221091	1105009	990968	900000
Date	9-2-2022	10-2-2022	11-2-2022	12-2-2022	13-2-2022	14-2-2022
Active cases	786833	693839	606474	533102	450000	419148
Date	15-2-2022	16-2-2022	17-2-2022	18-2-2022	19-2-2022	20-2-2022
Active cases	366256	328933	288099	250000	220186	198128

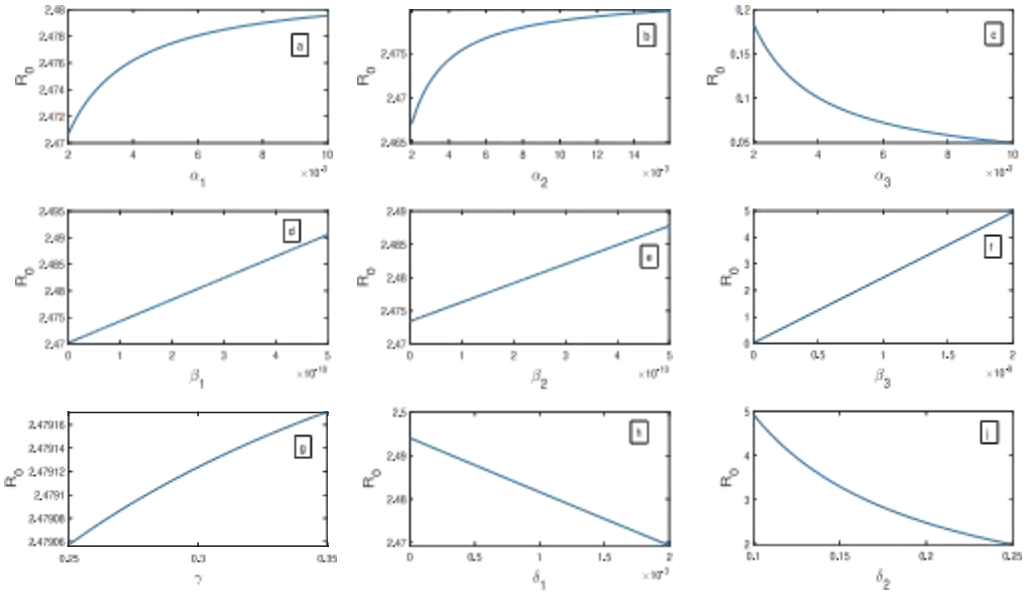

Fig. 14. The BRN R_0 plotted against (a) dose-1 vaccination rate α_1, (b) dose-2 vaccination rate α_2, (c) booster dose vaccination rate α_3, (d) disease transmission rate of non-vaccinated population β_1, (e) disease transmission rate of dose-1 vaccinated population β_2, (f) disease transmission rate of dose-2 vaccinated population β_3, (g) rate of exposed population who are asymptomatic γ, (h) rate of asymptomatic infected population become symptomatic to disease δ_1, (j) rate of asymptomatic infected population getting recovered δ_2.

follows: S_0 = 520000000, S_3 = 10000, E = 15000000, I_A = 15000000, and R = 5000. Table 6 summarises the real-time symptomatic infected populations from 29th December 2021 to 20th February 2022.

The infected population I_S of the model (1) fits well with the real confirmed infected cases in India from the Table 6 with the parameter values estimated as in the Table 3, as shown in Fig. 15(b).

The infected populations I_A and I_S of the model (1) decrease when the booster dose vaccination rate α_3 increases, as shown in Figs. 16(a) and 16(b). The asymptomatic infected population I_A and the symptomatic infected

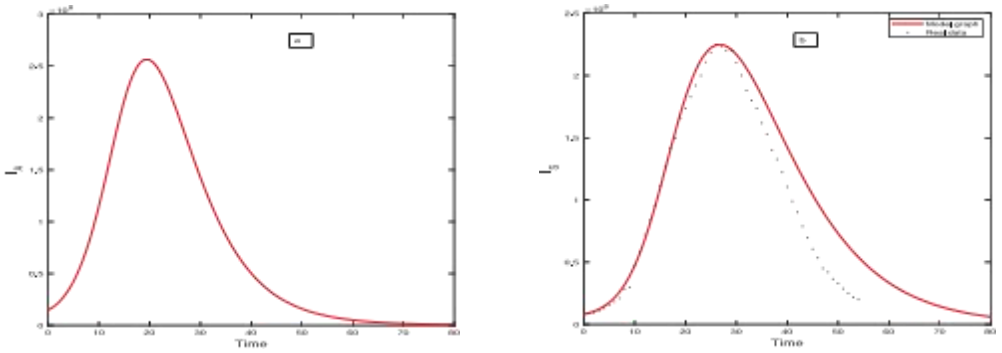

Fig. 15. Fitted with real data from Table 6 and values of parameters from Table 3, plot of (a) asymptomatic infected populations (I_A) and (b) symptomatic infected populations (I_S) against time t.

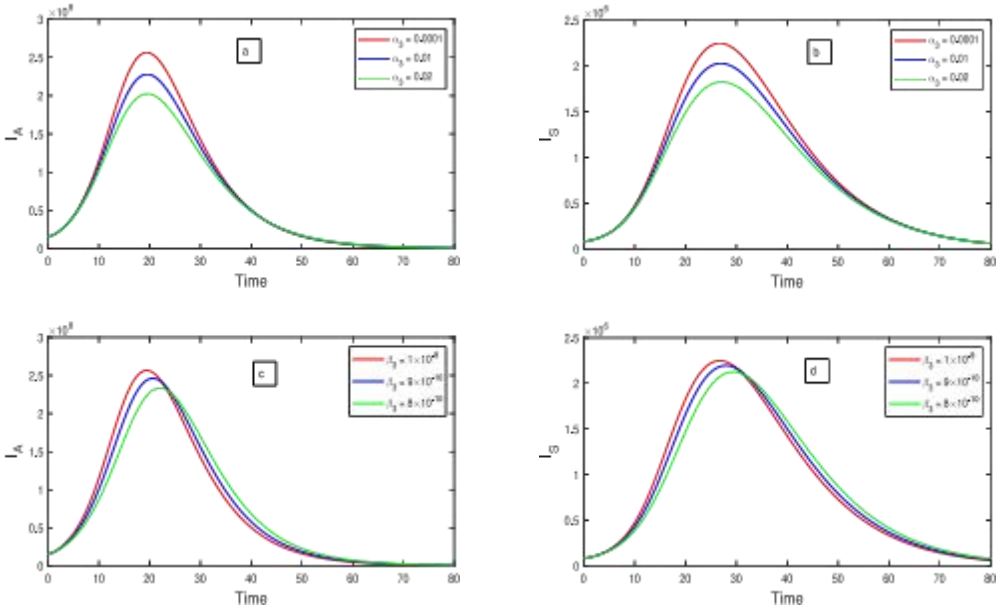

Fig. 16. A plot of the infected populations I_A and I_S over time various values of the booster dose vaccination rate α_3 among the dose-2 vaccinated susceptible population S_2 and disease transmission rate β_3 of dose-2 vaccinated susceptible population S_2.

population I_S steadily increase when the disease transmission rate β_3 among dose-2 vaccinated individuals increases, as shown in Figs. 16(c) and 16(d).

From Figs. 17(a) and 17(b), it is seen that the populationsI_A and I_S of the model (1) increase when the infection rate γ of the exposed individuals E increases. From Figs. 17(c) and 17(d), it is seen that the infected populations I_A and I_S of the model (1) are reduced when the rate of recovery δ_2 of theI_A population increases. Therefore, rapid recovery of the I_A population from the disease is crucial to reducing the rapid spread of the disease.

10. Conclusion

A COVID-19 mathematical model was developed for studying the disease transmission dynamics in India when a vaccination program is underway and the omicron variant of the coronavirus is dominant. According to the research, the Omicron system (1)'s DFE is LAS when the basic reproduction number is below one but unstable otherwise. The stability of the equilibrium points was tested after the basic reproduction number, R_0, was computed. The system (1) exhibits forward bifurcation at $R_0 = 1$ when $a < 0$(38). The sensitivity parameters were calculated using the notion of normalised forward sensitivity. The time-series graphs for various populations with assumed parameter

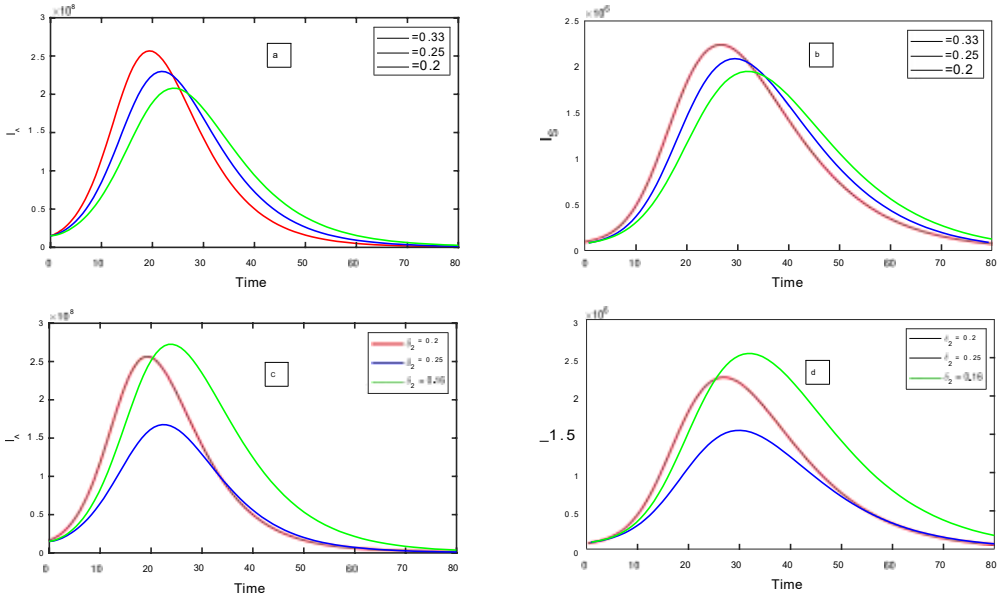

Fig. 17. For different values of the infection rate γ and the recovered rate from the disease of asymptomatic infected persons δ_2, a time-series graph of asymptomatic infected and symptomatic infected populations is shown.

values are created in the numerical analysis section to validate the results of the stability theorems. Different model parameters are determined based on current omicron variant transmission among various susceptible populations, divided into groups based on vaccination dosage. The estimated values are used to examine variations in the value of the threshold parameter, R_0, to the model's most essential parameters. The sensitivity analysis is performed, and the most sensitive parameters are identified. The numerical experiments are carried out using estimated parameter values for real infected cases in the Indian population during the omicron variant virus transmission and vaccination drive in India, and it is found that the model (1)'s symptomatic infected population matches the real infected data well. Finally, some of the key estimated parameters are examined using time series graphs of the model (1)'s infected populations. In future research, we will look at this model with a non-human reservoir compartment for the omicron virus, investigate its dynamics, and compare the results to real-world data.

References

[1] 2020. Available online: https://www.who.int/emergencies/diseases/novel-coronavirus-2019/media-resources/news. (Assessed 19 June 2020).

[2] 2021. Available online: http://www.protezionecivile.gov.it/en/. (Accessed 10 April 2021).

[3] 2021. Available online: http://www.salute.gov.it/portale/home.html. (Accessed 10 April 2021).

[4] 2021. Available online: https://www.iss.it/en/. (Accessed 10 April 2021).

[5] Available online: https://pib.gov.in/Pressreleaseshare.aspx?PRID=1712710.

[6] Available online: https://cdsco.gov.in/opencms/opencms/en/biologicals/Vaccines/. (Accessed 23 March 2022).

[7] Available online: https://pib.gov.in/Pressreleaseshare.aspx?PRID=1645363.

[8] Available online: https://www.who.int/india/news/feature-stories/detail/india-rolls-out-the-world-s-largest-COVID-19-vaccination-drive.

[9] Available online: https://www.who.int/en/activities/tracking-SARS-CoV-2-variants.

[10] https://www.who.int/docs/default-source/gho-documents/world-health-statistic-reports/6-june-18108-world-health-statistics-2018.pdf.

[11] https://www.unicef.org/india/key-data.

[12] 2021. Available online: https://www.cdc.gov/mmwr/volumes/70/wr/mm705152e3.htm. (Accessed 31 December 2021).

[13] https://www.livemint.com/news/india/how-long-does-it-take-to-recover-from-omicron-centre-reveals-data-11642682192151.html.

[14] H.I. Abdel-Gawad, A.H. Abdel-Gawad, Discrete and continuum models of COVID-19 virus, formal solutions, stability and comparison with real data, Math. Comput. Simulation 190 (2021) 222–230.

[15] Hamdy I. Abdel-Gawad, Ahmed H. Abdel-Gawad, Discrete and continuum models of COVID-19 virus, formal solutions, stability and comparison with real data, Math. Comput. Simulation 190 (2021) 222–230.

[16] Z. Abreu, G. Cantin, C.J. Silva, Analysis of a COVID-19 compartmental model: A mathematical and computational approach, Math. Biosci. Eng. 18 (6) (2021) 7979–7998.

[17] Eduardo Acosta-González, Julián Andrada-Félix, Fernando Fernández-Rodríguez, On the evolution of the COVID-19 epidemiological parameters using only the series of deceased. A study of the Spanish outbreak using genetic algorithms, Math. Comput. Simulation 197 (2022) 91–104.

[18] D. Adak, A. Majumder, N. Bairagi, Mathematical perspective of COVID-19 pandemic: Disease extinction criteria in deterministic and stochastic models, Chaos Solitons Fractals 142 (2021).

[19] A. Alla Hamou, E. Azroul, A. Lamrani Alaoui, Fractional model and numerical algorithms for predicting COVID-19 with isolation and quarantine strategies, Int. J. Appl. Comput. Math. 7 (4) (2021).

[20] A.E.S. Almocera, G. Quiroz, E.A. Hernandez-Vargas, Stability analysis in COVID-19 within-host model with immune response, Commun. Nonlinear Sci. Numer. Simul. 95 (2021).

[21] M. Amouch, N. Karim, Modeling the dynamic of COVID-19 with different types of transmissions, Chaos Solitons Fractals 150 (2021).

[22] J. Andersson, S. Ghersheen, V. Kozlov, V.G. Tkachev, U. Wennergren, Effect of density dependence on coinfection dynamics, Anal. Math. Phys. 11 (4) (2021).

[23] S.S. Askar, Dipankar Ghosh, P.K. Santra, Abdelalim A. Elsadany, G.S. Mahapatra, A fractional order SITR mathematical model for forecasting of transmission of COVID-19 of India with lockdown effect, Results Phys. 24 (2021) 104067.

[24] M.A. Aziz-Alaoui, F. Najm, R. Yafia, Siard model and effect of lockdown on the dynamics of COVID-19 disease with non total immunity, Math. Model. Nat. Phenom. 16 (2021).

[25] A. Babaei, M. Ahmadi, H. Jafari, A. Liya, A mathematical model to examine the effect of quarantine on the spread of coronavirus, Chaos Solitons Fractals 142 (2021).

[26] Shraddha Ramdas Bandekar, Mini Ghosh, A co-infection model on TB - COVID-19 with optimal control and sensitivity analysis, Math. Comput. Simulation 200 (2022) 1–31.

[27] Sanjoy Basu, R. Prem Kumar, P.K. Santra, G.S. Mahapatra, A.A. Elsadany, Preventive control strategy on second wave of COVID-19 pandemic model incorporating lock-down effect, Alex. Eng. J. (2022).

[28] C.M. Batistela, D.P.F. Correa, Á.M. Bueno, J.R.C. Piqueira, SIRSi compartmental model for COVID-19 pandemic with immunity loss, Chaos Solitons Fractals 142 (2021).

[29] C.F. Beards, 5 - automatic control systems, in: C.F. Beards (Ed.), Engineering Vibration Analysis with Application To Control Systems, Butterworth-Heinemann, 1995, pp. 171–279.

[30] T.A. Biala, Y.O. Afolabi, AQM Khaliq, How efficient is contact tracing in mitigating the spread of COVID-19? a mathematical modeling approach, Appl. Math. Model. 103 (2022) 714–730.

[31] Garrett Birkhoff, Gian-Carlo Rota, Ordinary Differential Equations, Vol. 4, Wiley New York, 1978.

[32] H. Bulut, M. Gölgeli, F.M. Atay, Modelling personal cautiousness during the COVID-19 pandemic: a case study for Turkey and Italy, Nonlinear Dynam. 105 (1) (2021) 957–969.

[33] Carlos Castillo-Chavez, Baojun Song, Dynamical models of tuberculosis and their applications, Math. Biosci. Eng. 1 (2) (2004) 361.

[34] C. Castillo Chavez, Z. Feng, W. Huang, On the computation of R0 and its role on global stability, in: Mathematical Approaches for Emerging and Re-Emerging Infection Diseases: An Introduction, Vol. 125, The IMA Volumes in Mathematics and Its Applications, 2002, pp. 31–65.

[35] Ziren Chen, Lin Feng, Harold A. Lay, Khaled Furati, Abdul Khaliq, SEIR model with unreported infected population and dynamic parameters for the spread of COVID-19, Math. Comput. Simulation 198 (2022) 31–46.

[36] Patricio Cumsille, Óscar Rojas-Díaz, Pablo Moisset de Espanés, Paula Verdugo-Hernández, Forecasting COVID-19 Chile'second outbreak by a generalized SIR model with constant time delays and a fitted positivity rate, Math. Comput. Simulation 193 (2022) 1–18.

[37] P. Das, S.S. Nadim, S. Das, P. Das, Dynamics of COVID-19 transmission with comorbidity: a data driven modelling based approach, Nonlinear Dynam. 106 (2) (2021) 1197–1211.

[38] M. De La Sen, A. Ibeas, A. Garrido, On a new SEIRDE oi oepidemic model eventually initiated from outside with delayed re-susceptibility and vaccination and treatment feedback controls, Phys. Scr. 96 (9) (2021).

[39] O.L. De Silva, S. Lasaulce, I.-C. Morarescu, On the efficiency of decentralized epidemic management and application to COVID-19, IEEE Control Syst. Lett. 6 (2022) 884–889.

[40] M.L. Diagne, H. Rwezaura, S.Y. Tchoumi, J.M. Tchuenche, A mathematical model of COVID-19 with vaccination and treatment, Comput. Math. Methods Med. 2021 (2021).

[41] H.A.A. El-Saka, A. Al-Dmour, I. Obaya, Asymptomatic and pre-symptoms transmission of COVID-19 in heterogeneous epidemic network, Inf. Sci. Lett. 11 (1) (2022) 149–160.

[42] L.L. Elías, S.L. Elías, A.M. del Rey, An analysis of contact tracing protocol in an over-dispersed SEIQR COVID-like disease, Physica A 590 (2022).

[43] José Enrique Amaro, Jérémie Dudouet, José Nicolás Orce, Global analysis of the COVID-19 pandemic using simple epidemiological models, Appl. Math. Model. 90 (2021) 995–1008.

[44] D.J. Fotsa-Mbogne, S.Y. Tchoumi, Y. Kouakep-Tchaptchie, V.C. Kamla, J.-C. Kamgang, D.E. Houpa-Danga, S. Bowong-Tsakou, D. Bekolle, Estimation and optimal control of the multiscale dynamics of COVID-19: a case study from Cameroon, Nonlinear Dynam. 106 (3) (2021) 2703–2738.

[45] H.B. Fredj, F. Chérif, Novel corona virus disease infection in Tunisia: Mathematical model and the impact of the quarantine strategy, Chaos Solitons Fractals 138 (2020).

[46] K.M. Furati, I.O. Sarumi, A.Q.M. Khaliq, Fractional model for the spread of COVID-19 subject to government intervention and public perception, Appl. Math. Model. 95 (2021) 89–105.

[47] S.M. Garba, J.M.-S. Lubuma, B. Tsanou, Modeling the transmission dynamics of the COVID-19 pandemic in South Africa, Math. Biosci. 328 (2020).

[48] A. George Maria Selvam, J. Alzabut, D. Abraham Vianny, M. Jacintha, F.B. Yousef, Modeling and stability analysis of the spread of novel coronavirus disease COVID-19, Int. J. Biomath. 14 (5) (2021).

[49] Jayanta Kumar Ghosh, Sudhanshu Kumar Biswas, Susmita Sarkar, Uttam Ghosh, Mathematical modelling of COVID-19: A case study of Italy, Math. Comput. Simulation 194 (2022) 1–18.

[50] D. Ghosh, P.K. Santra, G.S. Mahapatra, Amr Elsonbaty, A.A. Elsadany, A discrete-time epidemic model for the analysis of transmission of COVID19 based upon data of epidemiological parameters, Eur. Phys. J. Spec. Top. (2022) 1–10.

[51] G. Gonzalez-Parra, A.J. Arenas, Qualitative analysis of a mathematical model with presymptomatic individuals and two SARS-CoV-2 variants, Comput. Appl. Math. 40 (6) (2021).

[52] S.M. Kassa, J.B.H. Njagarah, Y.A. Terefe, Analysis of the mitigation strategies for COVID-19: From mathematical modelling perspective, Chaos Solitons Fractals 138 (2020).

[53] S. Khajanchi, K. Sarkar, Forecasting the daily and cumulative number of cases for the COVID-19 pandemic in India, Chaos 30 (7) (2020).

[54] O. Khyar, K. Allali, Global dynamics of a multi-strain SEIR epidemic model with general incidence rates: application to COVID-19 pandemic, Nonlinear Dynam. 102 (1) (2020) 489–509.

[55] R. Prem Kumar, Sanjoy Basu, P.K. Santra, D. Ghosh, G.S. Mahapatra, Optimal control design incorporating vaccination and treatment on six compartment pandemic dynamical system, Results Control Optim. (2022) 100115.

[56] Joseph P. La Salle, The Stability of Dynamical Systems, SIAM, 1976.

[57] A. Labzai, A. Kouidere, O. Balatif, M. Rachik, Stability analysis of mathematical model new corona virus (COVID-19) disease spread in population, Commun. Math. Biol. Neurosci. 2020 (2020) 1–19.

[58] U. Avila-Ponce de León, Á.G.C. Pérez, E. Avila-Vales, An SEIARD epidemic model for COVID-19 in Mexico: Mathematical analysis and state-level forecast, Chaos Solitons Fractals 140 (2020).

[59] Jijun Liu, Liyan Wang, Qiang Zhang, Shing-Tung Yau, The dynamical model for COVID-19 with asymptotic analysis and numerical implementations, Appl. Math. Model. 89 (2021) 1965–1982.

[60] B.K. Mishra, A.K. Keshri, D.K. Saini, S. Ayesha, B.K. Mishra, Y.S. Rao, Mathematical model, forecast and analysis on the spread of COVID-19, Chaos Solitons Fractals 147 (2021).

[61] C.N. Ngonghala, E. Iboi, S. Eikenberry, M. Scotch, C.R. MacIntyre, M.H. Bonds, A.B. Gumel, Mathematical assessment of the impact of non-pharmaceutical interventions on curtailing the 2019 novel coronavirus, Math. Biosci. 325 (2020).

[62] N.I. Okposo, M.O. Adewole, E.N. Okposo, H.I. Ojarikre, F.A. Abdullah, A mathematical study on a fractional COVID-19 transmission model within the framework of nonsingular and nonlocal kernel, Chaos Solitons Fractals 152 (2021).

[63] Debkumar Pal, D. Ghosh, P.K. Santra, G.S. Mahapatra, Mathematical modeling and analysis of COVID-19 infection spreads in India with restricted optimal treatment on disease incidence, Biomath 10 (1) (2021) ID–2106147.

[64] D. Pal, D. Ghosh, P.K. Santra, G.S. Mahapatra, Mathematical modeling and analysis of COVID-19 infection spreads with restricted optimal treatment of disease incidence, Biomath 10 (1) (2021).

[65] V.S. Panwar, P.S. Sheik Uduman, J.F. Gómez-Aguilar, Mathematical modeling of coronavirus disease COVID-19 dynamics using CF and ABC non-singular fractional derivatives, Chaos Solitons Fractals 145 (2021).

[66] O. Postavaru, S.R. Anton, A. Toma, COVID-19 pandemic and chaos theory, Math. Comput. Simulation 181 (2021) 138–149.

[67] R. Prem Kumar, Sanjoy Basu, Dipankar Ghosh, Prasun Kumar Santra, G.S. Mahapatra, Dynamical analysis of novel COVID-19 epidemic model with non-monotonic incidence function, J. Public Affairs (2021) e2754.

[68] S. Rezapour, H. Mohammadi, M.E. Samei, SEIR epidemic model for COVID-19 transmission by Caputo derivative of fractional order, Adv. Difference Equ. 2020 (1) (2020).

[69] P. Samui, J. Mondal, S. Khajanchi, A mathematical model for COVID-19 transmission dynamics with a case study of India, Chaos Solitons Fractals 140 (2020).

[70] M. Serhani, H. Labbardi, Mathematical modeling of COVID-19 spreading with asymptomatic infected and interacting peoples, J. Appl. Math. Comput. 66 (1–2) (2021).

[71] A.S. Shaikh, I.N. Shaikh, K.S. Nisar, A mathematical model of COVID-19 using fractional derivative: outbreak in India with dynamics of transmission and control, Adv. Difference Equ. 2020 (1) (2020).

[72] M.Q. Shakhany, K. Salimifard, Predicting the dynamical behavior of COVID-19 epidemic and the effect of control strategies, Chaos Solitons Fractals 146 (2021).

[73] Wutiphol Sintunavarat, Ali Turab, Mathematical analysis of an extended SEIR model of COVID-19 using the ABC-fractional operator, Math. Comput. Simulation 198 (2022) 65–84.

[74] S.Y. Tchoumi, M.L. Diagne, H. Rwezaura, J.M. Tchuenche, Malaria and COVID-19 co-dynamics: A mathematical model and optimal control, Appl. Math. Model. 99 (2021) 294–327.

[75] A.W. Tesfaye, T.S. Satana, Stochastic model of the transmission dynamics of COVID-19 pandemic, Adv. Difference Equ. 2021 (1) (2021).

[76] N.H. Tuan, H. Mohammadi, S. Rezapour, A mathematical model for COVID-19 transmission by using the Caputo fractional derivative, Chaos Solitons Fractals 140 (2020).

[77] J. Waku, K. Oshinubi, J. Demongeot, Maximal reproduction number estimation and identification of transmission rate from the first inflection point of new infectious cases waves: COVID-19 outbreak example, Math. Comput. Simulation 198 (2022) 47–64.

[78] Yingkang Xie, Zhen Wang, Transmission dynamics, global stability and control strategies of a modified SIS epidemic model on complex networks with an infective medium, Math. Comput. Simulation 188 (2021) 23–34.

[79] P. Yarsky, Using a genetic algorithm to fit parameters of a COVID-19 SEIR model for US states, Math. Comput. Simulation 185 (2021) 687–695.

[80] H.M. Youssef, N.A. Alghamdi, M.A. Ezzat, A.A. El-Bary, A.M. Shawky, A new dynamical modeling SEIR with global analysis applied to the real data of spreading COVID-19 in Saudi Arabia, Math. Biosci. Eng. 17 (6) (2020) 7018–7044.

[81] H. Youssef, N. Alghamdi, M.A. Ezzat, A.A. El-Bary, A.M. Shawky, Study on the SEIQR model and applying the epidemiological rates of COVID-19 epidemic spread in Saudi Arabia, Infectious Disease Modelling 6 (2021) 678–692.

[82] Hongjun Zhu, Yan Li, Xuelian Jin, Jiangping Huang, Xin Liu, Ying Qian, Jindong Tan, Transmission dynamics and control methodology of COVID-19: a modeling study, Appl. Math. Model. 89 (2021) 1983–1998.

[83] C.-C. Zhu, J. Zhu, Dynamic analysis of a delayed COVID-19 epidemic with home quarantine in temporal-spatial heterogeneous via global exponential attractor method, Chaos Solitons Fractals 143 (2021).